Petroleum Science 21 (2024) 3815–3838

Contents lists available at ScienceDirect

Petroleum Science

journal homepage: www.keaipublishing.com/en/journals/petroleum-science

Original Paper

Control and prediction of bedding-parallel fractures in fine-grained sedimentary rocks: A case from the Permian Lucaogou Formation in Jimusar Sag, Junggar Basin, Western China

Zhao-Hui Zhang [a, b, *], Teng Zhang [c], Hua-Qing Liu [d], Xiang-Bo Li [d], Duo-Nian Xu [d, **]

[a] Xinjiang Key Laboratory for Geodynamic Processes and Metallogenic Prognosis of the Central Asian Orogenic Belt, Urumqi, 830046, Xinjiang, China
[b] School of Geology and Mining Engineering, Xinjiang University, Urumqi, 830046, Xinjiang, China
[c] YuanWangJingSheng Technology (Beijing) Co. Ltd., Beijing, 100083, China
[d] Northwest Branch, Research Institute of Petroleum Exploration and Development, PetroChina, Lanzhou, 730020, Gansu, China

ARTICLE INFO

Article history:
Received 24 August 2023
Received in revised form
28 March 2024
Accepted 4 September 2024
Available online 6 September 2024

Edited by Teng Zhu

Keywords:
Bedding-parallel fractures
Fine-grained sedimentary rocks
Multiscale matching
Quantitative prediction
Lucaogou formation
Junggar Basin

ABSTRACT

The fine-grained sedimentary rocks have numerous bedding-parallel fractures that are essential for the migration, enrichment, and efficient development of oil and gas. However, because of their variety and the complexity of the factors that affect them, their spatial prediction by the industrial community becomes challenging. Based on sample cores, thin sections, and well-logging and seismic data, this study employed a multi-scale data matching approach to quantitatively predict the development of bedding-parallel fractures and investigate their spatial distribution. Bedding-parallel fractures in the Lucaogou Formation in Jimusar Sag frequently occur along preexisting bedding planes and lithological interfaces. Unfilled bedding-parallel fractures inside or near source-rocks exhibit enhanced oil-bearing capacity. They were identified on micro-resistivity scanning images by the presence of regularly continuous black or nearly black sinusoidal curves. Overall, the developmental degree of bedding-parallel fractures was positively related to the brittle mineral and total organic carbon contents and negatively related to single reservoir interval thickness. The maintained porosity of the reservoir matrix contributed to a thorough response to factors affecting the development of bedding-parallel fractures. Here, an effective and objective method was proposed for predicting the development and distribution of bedding-parallel fractures in the fine-grained sedimentary rocks. The method was based on the matched reservoir interval density, reservoir interval density, and matched sweet spot density of bedding-parallel fractures. The prediction method integrated the significant advantages of high vertical resolution from logging curves and strong lateral continuity from seismic data. The average relative prediction error was 8% in the upper sweet spot in the Lucaogou Formation, indicating that the evaluation parameters for bedding-parallel fractures in fine-grained sedimentary rocks were reasonable and reliable and that the proposed prediction method has a stronger adaptability than the previously reported methods. The workflow based on multi-scale matching and stepwise progression can be applied in similar fine-grained sedimentary rocks, providing reliable technological support for the exploration and development of hydrocarbons.

1. Introduction

Fine-grained sedimentary rocks, characterized by grain sizes <0.0625 mm, function as both favorable reservoirs and source rocks (Aplin and Macquaker, 2011; Cao et al., 2016; Liu et al., 2019; Lin et al., 2021; Zeng et al., 2021, 2022). They are deposited in weak hydrodynamic settings and are primarily composed of clay minerals, terrigenous clasts, and authigenic carbonates (Krumbein,

* Corresponding author. Xinjiang Key Laboratory for Geodynamic Processes and Metallogenic Prognosis of the Central Asian Orogenic Belt, Urumqi, 830046, Xinjiang, China.
** Corresponding author.
E-mail addresses: zhangzhaohui@xju.edu.cn (Z.-H. Zhang), xu_dn@petrochina.com.cn (D.-N. Xu).

https://doi.org/10.1016/j.petsci.2024.09.003

1947; Ghadeer and Macquaker, 2011; Li et al., 2019; Pang et al., 2022). Recent studies have reported that fine-grained sedimentary rocks are well developed in the Junggar (Li et al., 2018; Shi et al., 2018; Ju et al., 2020), Ordos (Li et al., 2018; Shi et al., 2018; Ju et al., 2020), Songliao (Liu et al., 2019, 2021), and Bohaiwan (Wu et al., 2017; Zhao et al., 2019) basins in China. Extensive exploration and production activities in fine-grained sedimentary hydrocarbon reservoirs have revealed that natural fractures play key roles in improving the production capacity of hydrocarbon reservoirs (Gale et al., 2014; Luo et al., 2017; Zhang et al., 2017; Ju et al., 2020; Mohammed et al., 2021; Lai et al., 2022). Natural fractures that can considerably improve hydrocarbon storage, fluid flow, and productivity in fine-grained sedimentary rocks mainly include unfilled bedding-parallel fractures and opened tectonic fractures (McGinnis et al., 2017; Basa et al., 2019; Lai et al., 2022; Du et al., 2023b). Bedding-parallel fractures are fractures found along weak bedding interfaces and are extensively developed in fine-grained sedimentary layered rocks (Li et al., 2018; Abuamarah et al., 2019; Nabawy et al., 2020; Lai et al., 2022; Zeng et al., 2024). The formation mechanisms of bedding-parallel fractures have been revealed in diverse petroliferous basins; these mechanisms mainly include structural stress (Bergbauer and Pollard, 2004; Gale et al., 2014), hydrocarbon generation and expulsing acid dissolution (Lacombe et al., 2011; Wang et al., 2021), and pressure fracturing of authigenic fluids (Parnell et al., 1996; Feng and Chen, 2015). So far, the character description, stages, recognition, and developmental degree of bedding-parallel fractures have been examined with outcrop geological surveys, core observations, thin sections, and other methods (Ma et al., 2016; Zhao et al., 2019; Gu et al., 2020; Lu et al., 2021; Pang et al., 2022). However, relatively fewer studies have been conducted on systematic analysis of the factors affecting bedding-parallel fractures and geophysical spatial prediction of their development. So, it is necessary to both identify the factors affecting natural fracture development and quantitatively predict their distribution.

Well-logging data calibrated by core samples have been applied in bedding-parallel fractures, and several identification and evaluation methods have also been developed (Folkestad et al., 2012; Espejel et al., 2020; Zhang et al., 2020, 2022; Lai et al., 2022). Several quantitative parameters, such as the linear density and aperture of bedding-parallel fractures, have been established. Various application cases in diverse petroliferous basins have revealed the effectiveness of these parameters in evaluating bedding-parallel fractures (Schulz et al., 2005; Huang et al., 2006; Qu et al., 2016; Zhang et al., 2018, 2022; Lu et al., 2021; Xu et al., 2021; Zeng et al., 2021, 2022; Lai et al., 2022; Du et al., 2023a); however, these are difficult to use for seismic prediction owing to the differences in data resolution among the core samples, logging curve, and seismic events (Lai et al., 2015; Bhattacharya and Mishra, 2018; Lu et al., 2023). Although robust lateral continuous seismic data can be used for predicting the development of bedding-parallel fractures, obtaining compatible parameters at an appropriate scale remains challenging (Wei et al., 2021; Dong et al., 2022; Bao et al., 2023). Hence, it is necessary to bridge these gaps based on multi-scale geophysical information. Additionally, Various complex factors contribute to distinct differences in the development of bedding-parallel fractures in fine-grained sedimentary rocks, which also promote or weaken each other (Zhang et al., 2017; Lai et al., 2022; Pang et al., 2022; Liu et al., 2023). Unfortunately, only few studies have elucidated the relationship between the degree of the development of bedding-parallel fractures and intrinsic reservoir factors (e.g., mineralogical composition, lithology, reservoir thickness, and total organic carbon contents); accordingly, it is difficult to quantitatively predict the spatial distribution of the development of bedding-parallel fractures (Lai et al., 2022; Zeng et al., 2022). Therefore, methods for the multi-scale quantitative characterization and prediction of bedding-parallel fracture development in fine-grained sedimentary rocks should be comprehensively consider these affecting factors and practical applications.

The Lucaogou Formation in the Jimusar Sag exhibits considerable potential as fine-grained sedimentary hydrocarbon reservoirs (e.g., tight oil and shale oil), developed numerous parallel-bedding fractures, and is the key exploration interest in the Xinjiang Oilfield of PetroChina (Kuang et al., 2019; Pang et al., 2022; Zhang et al., 2022). When the formation of these fractures is temporally coupled with the hydrocarbon generation from the source rocks and the bedding fractures are spatially coupled with the source rocks, they show the best oil-bearing property (Yang et al., 2018; Kuang et al., 2019; Lu et al., 2021; Pang et al., 2022; Zhang et al., 2022; Chen et al., 2023). Recently, several wells in the Lucaogou Formation within the Jimusar Sag have achieved commercial petroleum flows from fine-grained sedimentary reservoirs characterized by the presence of a large number of bedding-parallel fractures. Subsequently, remarkable discoveries have been made in sedimentary settings, the formation mechanisms of bedding-parallel fractures, reservoir characteristics, and oil accumulation. These findings provide valuable references for predicting the development of bedding-parallel fractures. This study is primarily divided into two sections. The first section establishes a quantitative method for predicting the development of bedding-parallel fractures based on the proposed multi-scale characterization parameters, while the second section explores the factors affecting the development of bedding-parallel fracture development by evaluating the degree of development of these fractures. This study proposes an effective, objective, and practical method for predicting the development of bedding-parallel fractures in fine-grained sedimentary rocks and provides an important reference for application in other regions.

2. Geological settings

The Jimusar Sag (1300 km^2), formed on middle Carboniferous folded basement, is located in the south-eastern Junggar Basin in western China (Fig. 1(a)) and has experienced successive Hercynian, Indosinina, Yanshan, and Himalayan tectonic movements (Qiu et al., 2016; Kuang et al., 2012, 2019; Wu et al., 2019). Its current structural pattern comprises an asymmetric dustpan-like sag, faulting in the west and overlying in the east, with a half-ring belt monocline structure and rare faulting inside (Fig. 1(b) and (d)).

Continental fine-grained sedimentary rocks (e.g., tight oil and shale oil) of the Lucaogou Formation in the Jimusar Sag have been recently shown to have abundant hydrocarbon resources and remarkable exploration potential (Cao et al., 2016; Kuang et al., 2019; Zhi et al., 2019; Wang et al., 2020; Lin et al., 2021). Existing drilling, well-logging, and 3D seismic data have revealed the following stratigraphic sequence above the Carboniferous folded basement from the bottom to the top (Xiang et al., 2013): the Carboniferous (C) formation; the Jiangjunmiao (P_2j), Lucaogou (P_2l), and Wutonggou (P_3wt) Permian formations; the Jiucaiyuanzi (T_1j) Triassic formation; the Badaowan (J_1b) Jurassic formation; the Tugulu (K_1tg) Cretaceous formation, and Paleogene (E) formation (Fig. 1d). The lithological and electrical characteristics of the Lucoagou Formation, developed with 2.5 third-order cycles, were systematically analyzed, leading to its classification into the P_2l_1 and P_2l_2 sub-members (Fig. 1c) (Kuang et al., 2012; Yang et al., 2018; Pang et al., 2022). Two sweet spots were identified—the upper sweet spot in the P_2l_2 sub-member and the lower sweet spot in the P_2l_1 sub-member (Zhi et al., 2019; Lu et al., 2021; Lai et al., 2022). The abundance of industrial shale oil in these sub-members has

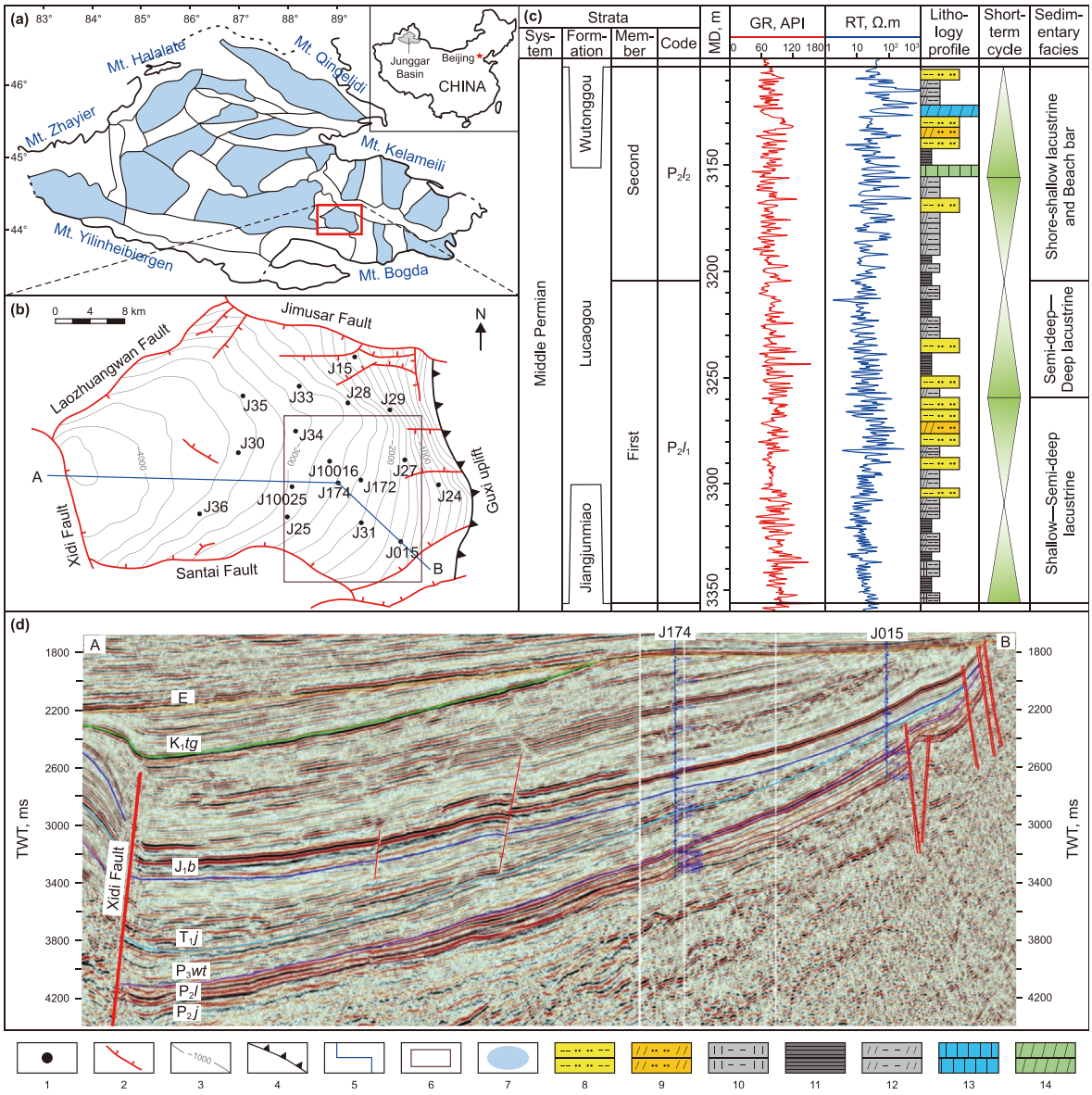

Fig. 1. Location and geological map of the Jimusar Sag in the Junggar Basin. **(a)** Simplified structural units of the Junggar Basin and location of the Jimusar Sag. **(b)** Structure contour of the top of the Lucaogou Formation of the Jimusar Sag. **(c)** Stratigraphic column of the Permian Lucaogou Formation in the Jimusar Sag. **(d)** Geological seismic profile in the east–west direction. Legend as follows: (1) wells, (2) faults, (3) Lucaogou Formation top structure contour in meters, (4) pinchout line of Lucaogou Formation, (5) seismic profile, (6) 3D seismic data volume survey, (7) subsag in Junggar Basin, (8) muddy siltstone, (9) dolomitic siltstone, (10) calcareous siltstone, (11) shale, (12) dolomitic mudstone, (13) limestone, (14) dolomite. GR: Natural gamma ray. RT: deep resistivity log. TWT: two-way travel time.

attracted considerable interest in China, leading to the construction of a national continental shale oil demonstration site.

The Lucaogou Formation, comprising typical fine-grained sedimentary rocks, with a thickness ranging from 100 to 350 m, is categorized as a saline lake with shore-shallow to deep lacustrine facies in a sedimentary environment (Fig. 1c) (Kuang et al., 2012; Yang et al., 2018; Zhi et al., 2019; Lin et al., 2021; Pang et al., 2022). Influenced by structural activities, climate, and sediment supply, the Lucaogou Formation displays a changing setting of deep and shallow lacustrine and extensively developed siltstones, carbonates, mudstones, and shales (Zhang et al., 2019; Lu et al., 2021; Lai et al., 2022; Pang et al., 2022). Owing to the periodic injection of terrestrial clastic material, the Lucaogou Formation mainly developed a thin sand layer with individual thickness ranging from 0.5 to 2 m and an accumulative thickness ranging from 20 to 90 m. The pore spaces in this layer mainly include intragranular dissolution pores, intergranular pores, and micro-fractures (Zhang et al., 2018; Pang et al., 2022; Zeng et al., 2022), characterized by a low matrix porosity and ultra-low permeability. The matrix porosity of rocks is primarily concentrated in the range of 0.1–24.8%, with a median value of 7.76%, whereas permeability is mainly distributed in the range of 0.004–9.82 mD, with a median of 0.4 mD (Fig. 2).

3. Materials and methodology

3.1. Material and photographic analysis

Cores, conventional logging curves, micro-resistivity scanning imaging images, 3D seismic data and scanning electron microscopy images, and thin section photographs from the Lucaogou Formation were used in this study. Geological data were obtained from the Xinjiang branch Oilfield Company of China National Petroleum

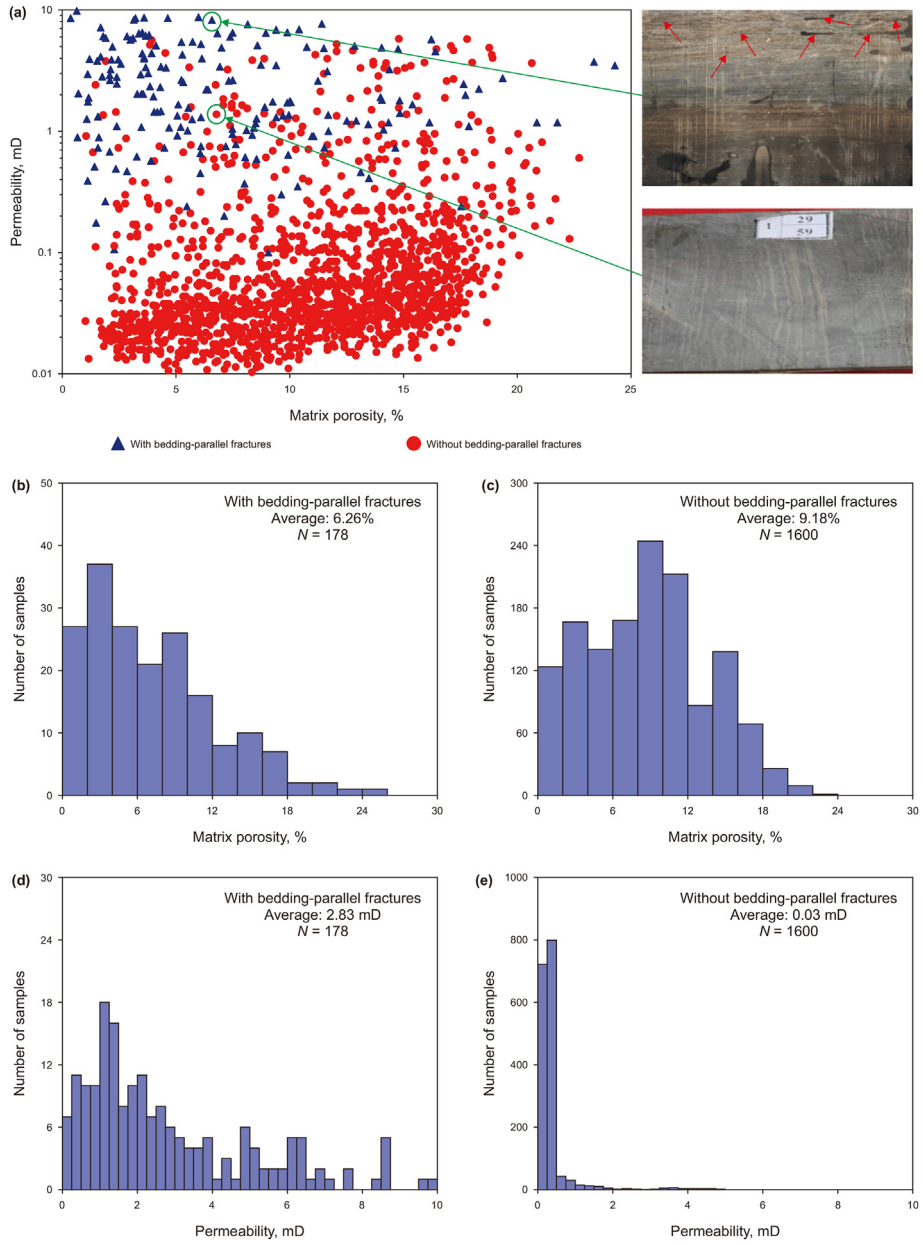

Fig. 2. Permeability and matrix porosity characteristics of the two groups (with bedding-parallel fractures and without bedding-parallel fractures) in the fine-grained sedimentary rocks of the Lucaogou Formation in the Jimusar Sag. **(a)** For each group, the cross plots showed a poor correlation between permeability and matrix porosity. **(b)** and **(c)** Matrix porosity distribution histogram of each group. **(d)** and **(e)** Permeability distribution histogram of each group.

Corporation and Zhundong Petroleum Technology Co., Ltd.

3.1.1. Core samples

In this study, 823 m drilled cores from five coring wells (J172, J174, J29, J10016, and J10025) were examined (Fig. 1(b)). Core samples were first examined to reveal fracture types, including diagenetic fractures (bedding-parallel fractures, dissolved fractures), tectonic fractures, and abnormal pressure fractures, as well as the filling characteristics of the fracture planes. They were then used to calibrate the micro-resistivity scanning imaging images and identify geological variables of interest (Moreau and Joubert, 2016; Zhang et al., 2020; Lai et al., 2022).

3.1.2. Geophysical datasets

Conventional wireline logs at 0.125 m intervals were acquired from 27 wells. Natural gamma ray (GR), spontaneous potential (SP), density (DEN), acoustic velocity (AC), compensated neutron log (CNL), true formation resistivity (RT), flushed zone resistivity (RXO), and invaded zone resistivity (RI) were primarily used to evaluate reservoir properties (e.g., lithology, porosity, thickness, oil layer types) by applying cross plots and mathematical physical models (Lai et al., 2017).

Micro-resistivity scanning images from 27 wells, with a longitudinal resolution of 5 mm, revealed continuously fine features of the wellbore wall, evidenced by color variations (0–255) presented in static and dynamic images (Serra, 1989; Rajabi et al., 2010; Moreau and Joubert, 2016; Zhang et al., 2020; Lai et al., 2022). Static images were normalized across the entire interval, encompassing the entire Lucaogou Formation, and were useful in identifying lithology. Contrastingly, dynamic images, which are scaled in the

sliding window (usually 0.6096 m), provided specific data on the geological characteristics of the borehole (Donselaar and Schmidt, 2005; Wilson et al., 2013; Keeton et al., 2015; Moreau and Joubert, 2016; Aghliet al., 2020; Zhang et al., 2020; Lai et al., 2022; Pang et al., 2022), such as grain size, sedimentary beddings, fractures, and vugs.

The 3D seismic data (28 Hz dominant-frequency) were acquired in situ and provided reliable information for the prediction of the development of bedding-parallel fractures. The selected study area, spanning approximately 250 km^2, was located in the eastern Jimusar Sag (Fig. 1(b)).

3.1.3. Petrographic analysis

Thin section photographs and scanning electron microscopic (SEM) images can provide fine micro-images (nanometer to micrometer scale) of microfractures (<0.1 mm), thereby characterizing fine microfractures (Loucks et al., 2009; Gou et al., 2019; Espejel et al., 2020; Lin et al., 2021; Zhu, 2021). Over 40 polished thin section photographs gathered from five drilled boreholes in the Jimusar Sag were studied using petrographic optical microscopy to distinguish microfractures. Additionally, SEM images obtained from 74 samples, using an accelerating voltage of 20 kV, were also used to identify microfractures.

3.2. Methodology

The fine-grained sedimentary rocks studied exhibit low matrix porosity, strong heterogeneity, and bedding-parallel fracture development (Yang et al., 2018; Zhang et al., 2018; Lu et al., 2021; Pang et al., 2022). Quantitatively characterizing reservoir bedding-parallel fractures using sample cores and FMI images is simple (Zhang et al., 2020; Lai et al., 2022; Pang et al., 2022). However, these methods cannot be directly used to predict the macro distribution of bedding-parallel fractures without seismic data. To address this issue and predict the development characteristics of bedding-parallel fractures in fine-grained sedimentary rocks, special attention was paid to their identification and quantitative characterization as well as the multi-scale integrated application of seismic, FMI, and conventional logging data.

3.2.1. Mathematical model

Matrix porosity and oil saturation were calculated using conventional logging curves calibrated using the core samples. Additionally, individual oil layer types were identified, and their layer thickness was estimated (Lai et al., 2017; Zhang et al., 2022). Oil layers with better oil-bearing characteristics were identified and evaluated based on the matrix porosity and oil saturation, which were calculated from conventional logging curves. The identification criteria for oil layers were as follows: matrix porosity >7%, oil saturation >70%, and thickness >0.5 m. Subsequently, these oil layers were divided into four ranks based on their oil saturation levels. The oil saturation values falling in the ranges of 70%–75%, 75%–80%, and 80%–85% and >85% were categorized as class IV, III, II, and I types of oil layers, respectively. The identification of these oil layer types was automatically completed using a code developed employing the CIFLog software. These oil layers may be continuous or discontinuous in the longitudinal direction, which is represented with a stratigraphic model (Fig. 3). We observed that the AB oil layer was discontinuous, while the CD and DE oil layers were continuous. In this case, the AB and CE intervals were considered as a single reservoir interval, indicating that the single reservoir interval consisted of a discontinuous oil layer or several continuous oil layers.

The density of the bedding-parallel fractures within the reservoir interval was introduced to characterize the intensity of the development of bedding-parallel fractures based on the number of fractures and the thickness of the reservoir interval. Bedding-parallel fractures in fine-grained sedimentary rocks were identified, and the density of bedding-parallel fractures in a single reservoir interval was calculated using results interpreted from the conventional logging and FMI images. The parameters were calibrated using cores at specific depths to determine the empirical correction value (Zhang et al., 2022). Fig. 3 shows that the CE interval was a single reservoir interval comprising two oil layers (CD and DE intervals). In this case, the density of the bedding-parallel fractures in a single reservoir interval was $N_2 + N_3/H_2 + H_3$. Thus, the reservoir interval density of the bedding-parallel fracture was calculated using Eq. (1) as follows:

$$BFd_{RI} = \frac{\sum_{i=1}^{n} N_{OLi}}{\sum_{i=1}^{n} H_{OLi}} \tag{1}$$

where BFd_{RI} is the reservoir interval density of the bedding-parallel fracture, i is the number of oil layers in the reservoir interval ($i = 1, 2, 3, \ldots, n$), N_{OLi} is the subordinate oil layer bedding-parallel fracture number in the reservoir interval, and H_{OLi} is the subordinate oil layer thickness in the reservoir interval.

Selecting a reservoir interval density of bedding-parallel fractures is particularly crucial for predicting and evaluating the development of bedding-parallel fractures in fine-grained sedimentary rocks. Considering that the reservoir interval density of bedding-parallel fractures is clearly affected by matrix porosity (Chen et al., 2016; Zhang et al., 2017; Lu et al., 2021; Pang et al., 2022), the weighted porosity was used as an estimate of the reservoir interval porosity. The weighting coefficient was determined from the oil layer thickness in the reservoir interval. Fig. 3 shows that FK is a single reservoir interval, comprising three oil layers (FG, GJ, and JK intervals). In this case, the weighted matrix porosity of the single reservoir interval is $(H_4 \cdot \varphi_4 + H_5 \cdot \varphi_5 + H_6 \cdot \varphi_6)/(H_4 + H_5 + H_6)$. Eq. (2) was used to calculate the weighted matrix porosity as follows:

$$\varphi_{RI} = \frac{\sum_{i=1}^{n} H_{OLi} \cdot \varphi_{OLi}}{\sum_{i=1}^{n} H_{OLi}} \tag{2}$$

where ϕ_{RI} is the weighted matrix porosity of a reservoir interval and ϕ_{OLi} is the subordinate oil layer matrix porosity in the reservoir interval.

The 3D seismic data used to predict the distribution of reservoirs during oil and gas explorations worldwide have revealed that the identifiable thickness of reservoirs is considerably affected by the dominant frequency (Shang et al., 2021; Dong et al., 2022; Bao et al., 2023), which is theoretically greater than a quarter of the reflection wavelength. In this study, the thickness of a single reservoir interval predicted by seismic data was substantially larger than that obtained from logging curves (Fig. 3). Accordingly, a sweet spot interval revealed by sensitive seismic attributes may consist of several reservoir intervals interpreted from logging curves (Dong et al., 2022; Bao et al., 2023). In the stratigraphic model displayed in Fig. 3, the AQ sweet spot interval revealed by seismic attributes is composed of the AB, CE, FK, and PQ reservoir intervals obtained from conventional logging curves. Conventional average methods are unsuitable and not universally applicable for determining the conversion relationship between sweet spot and reservoir intervals using 2D scattered intersection charts. To resolve this issue,

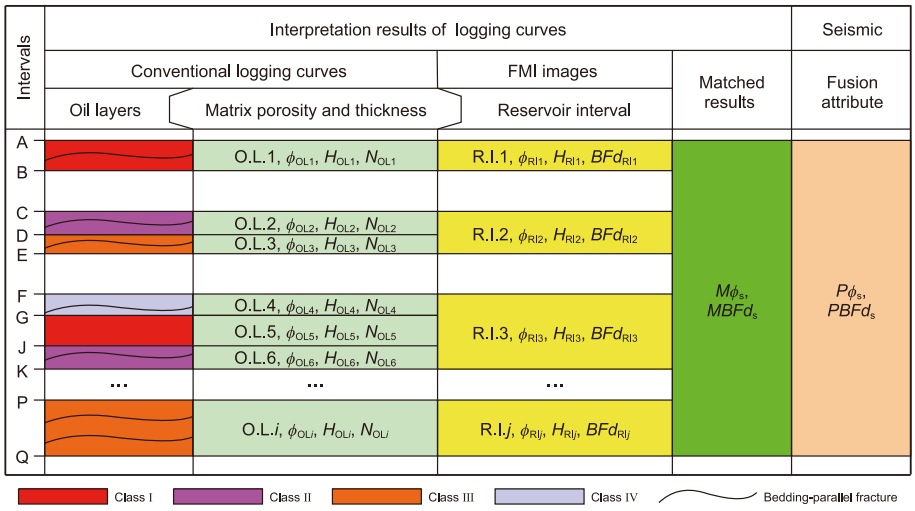

Fig. 3. Evaluation methods for quantitative characterization of bedding-parallel fractures based on conventional logs and FMI images. O.L.*i* is the *i*-th oil layer in a reservoir interval. ϕ_{OLi} and H_{OLi} denote the matrix porosity and thickness of the *i*-th oil layer, respectively. N_{OLi} is the numbers of bedding-parallel fractures in the *i*-th oil layer. R.I.*j* is the *j*-th reservoir interval in a sweet spot interval. ϕ_{RIj}, H_{RIj}, and BFd_{RIj} denote the weighted matrix porosity, accumulative thickness, and reservoir interval density of bedding-parallel fractures in the *j*-th reservoir interval. *i* is the number of oil layers in a reservoir interval ($i = 1, 2, 3, \ldots, n$). *j* is the number of reservoir intervals in a sweet spot interval ($j = 1, 2, 3, \ldots, m$). $M\phi_s$ and $MBFd_s$ denote the matched matrix porosity and sweet spot density of bedding-parallel fractures in a sweet spot interval, respectively. $P\phi_s$ and $PBFd_s$ denote the predicted matrix porosity and sweet spot density of bedding-parallel fractures in a sweet spot interval, respectively.

adjusting weight analysis was employed in this study. Adjusting weight analysis is a data matching method for calculating the reservoir parameters (e.g., matrix porosity, bedding-parallel fractures density) of sweet spot intervals using a fine synthetic seismogram, which is consistent with the objective elements and has reliable petrophysical basis in reservoir evaluation (Schulz et al., 2005; Xiao et al., 2015; Corina and Hovda, 2018; Zheng et al., 2021; D.M. Niu et al., 2022). Based on Fig. 3, Eqs. (3) and (4) were established as follows:

$$M\varphi_s = \frac{\sum_{j=1}^{m} H_{RIj} \cdot \varphi_{RIj}}{\sum_{j=1}^{m} H_{RIj}} \tag{3}$$

$$H_{RI} = \sum_{j=1}^{m} H_i \tag{4}$$

where $M\phi_s$ is the matched matrix porosity of the sweet spot interval, ϕ_{RIj} is the subordinate reservoir interval matrix porosity in the sweet spot interval, H_{RIj} is the subordinate reservoir interval thickness in the sweet spot interval, H_i is the subordinate oil layer thickness in the reservoir interval, and *j* is the number of reservoir intervals in the sweet spot interval ($j = 1, 2, 3, \ldots, m$).

$$MBFd_s = \frac{\sum_{j=1}^{m} BFd_{RIj} \cdot \varphi_{RIj}}{\sum_{j=1}^{m} \varphi_{RIj}} \tag{5}$$

where $MBFd_s$ is the matched sweet spot density of bedding-parallel fractures and BFd_{RIj} is the subordinate reservoir interval density of bedding-parallel fractures in a sweet spot interval.

Furthermore, based on the logging data of drilled exploratory wells, a statistical mathematical relationship between $M\phi_s$ and $MBFd_s$ was established using interpretation results of conventional logging and FMI images as follows:

$$MBFd_s = f(M\varphi_s) \tag{6}$$

where $f(M\phi_s)$ denotes a function relationship, such as linear, exponential, or power. To achieve the highest possible accuracy, the fitting correlation coefficient of the mathematical formula must be as large as possible (Corina and Hovda, 2018; Zheng et al., 2021), i.e., $E(MBFd_{sk} - f(M\varphi_{sk})) = 0$ and $\min(Var(MBFd_{sk} - f(M\varphi_{sk})))$, where *k* is the number of known points involved in the statistical datasets.

3.2.2. Artificial workflow

Based on the proposed logging parameters and calculating methods, the distribution of bedding-parallel fractures in fine-grained sedimentary rocks was quantitatively predicted using seismic and borehole data, multi-scale matching, and stepwise progression. The artificial workflow has been presented in Fig. 4, and the specific steps are as follows.

(1) Based on conventional logging curves and FMI images, all bedding-parallel fractures were identified, and the thickness and matrix porosity of each oil layer and reservoir interval, respectively, were calculated.
(2) Using the results of the first step, $M\phi_s$ and $MBFd_s$ were calculated.
(3) The functional relationship between $M\phi_s$ and $MBFd_s$ was fitted according to the mathematical statistical analysis method.
(4) An interwell matrix porosity model ($P\phi_s$) to predict the sweet spot density of bedding-parallel fractures was established by coupling the seismic attributes sensitive to $M\phi_s$.
(5) The planar distribution of the extent of the development of bedding-parallel fractures ($PBFd_s$) was predicted in fine-grained sedimentary rocks according to the $P\phi_s$.

As the selection of matrix porosity-sensitive seismic attributes, extraction of fusion-sensitive attributes, and acquisition of an interwell matrix porosity model can be easily achieved using commercial software (e.g., Strata, Jason, Landmark), these steps are not described here.

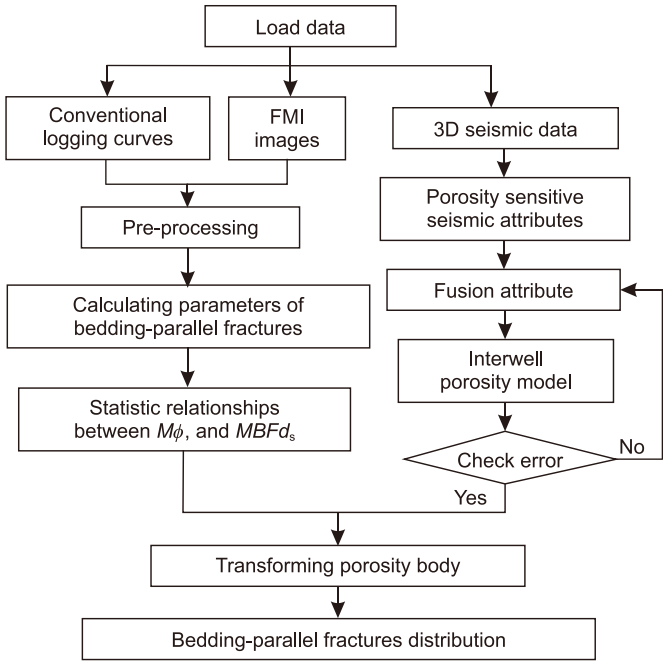

Fig. 4. The artificial workflow chart of multi-scale matching and step-by-step progressing method for predicting the development of bedding-parallel fractures.

4. Results

4.1. Multi-scale characteristics of bedding-parallel fractures

In the Permian Lucaogou Formation of the Jimusar Sag, bedding-parallel fractures are the most extensive diagenetic fractures (Zhang et al., 2018; Lu et al., 2021; Lai et al., 2022; Pang et al., 2022), which occur along sediment bedding planes that are weaker than rock matrix due to complicated mechanical compaction, weathering, solution, and tectonics (Bergbauer and Pollard, 2004; Gale et al., 2014; Zeng et al., 2022). A statistical analysis of these multi-scale characteristics of bedding-parallel fractures would provide a reliable basis for predicting their distribution.

4.1.1. Macroscopic characteristics of core samples

A total of 539 natural fractures were identified in 324 m drilled cores from the Lucaogou Formation. Among them, bedding-parallel fractures were usually observed at the interface of different lithologies or beddings, extending parallel or almost parallel to the interface planes (Fig. 5(a)–5(i)) (Zhang et al., 2018; Lai et al., 2022). They primarily exhibited horizontal or almost horizontal development through the core, variable aperture and gentle fractured plane characterization, and strong connectivity (Fig. 5(f)). Most bedding-parallel fracture planes were also found to be unfilled, with oil-saturated, oil-stained, and oil-potted phenomena often represented along the bedding-parallel fracture planes (Fig. 5(e), (f), and 5(h)). Affected by tectonic activities or diagenesis at differential stages, some bedding-parallel fracture planes were fully or partially filled with calcite, pelite, and other minerals (e.g., quartz, dolomite, asphalt) (Fig. 5(a)) (Zhang et al., 2019; Lai et al., 2022). Accordingly, the oil-bearing capacity was poor, with the fractures sometimes generating no oil (Lu et al., 2021; Pang et al., 2022). However, as certain filling minerals, such as calcite, can be dissolved by acidic solutions during the late-stage diagenetic modification, cementation and dissolution may occur within these bedding-parallel fracture planes (Fig. 5(d), (e), and 5(i)). Stylolite, which was formed by dissolution (Zhang et al., 2018; Lai et al., 2022; Pang et al., 2022; Zeng et al., 2022) and can be recognized from the serrated surfaces in the core samples, also appeared in the study area (Fig. 5(h) and (j)).

Compared with bedding-parallel fractures, tectonic fractures appeared at a regularly stable frequency, with a specific orientation constrained by tectonic trends—usually extending (Fig. 5(j) and (k)), and fracture dip angles mainly distributed between 60° and 80° (Fig. 10(b)). Additionally, some abnormal pressure fractures caused by overpressure fluid in the Lucaogou Formation (Zhang et al., 2019; Lai et al., 2022; Pang et al., 2022), which were commonly fully filled with calcite cements and irregularly distributed in vein groups, were also observed (Fig. 5(l)). These fractures were denoted as drainage fractures, which can be easily identified using core samples (Zhang et al., 2019; Lai et al., 2022).

4.1.2. Microscopic characteristics of thin sections and SEM images

Thin section photographs showed that the bedding-parallel fractures occurred within the bedding surfaces (Fig. 6(a) and (f)), usually bypassing the hard mineral particles (Fig. 6(a), (c), and 6(d)). Therefore, the visual geometry shapes of microfractures showed a curved extension, rather than a straight one, as shown on the core samples (Zhu, 2021; Pang et al., 2022). The morphology of microfractures resembled a wedge, with fracture apertures ranging from 0.1 to 5 μm and lengths ranging from 0.1 to 10 mm (Fig. 6(a)–6(g)). In cases where dissolution had occurred along the bedding-parallel fracture planes during the late-stage diagenetic modification (Fig. 6(g)), the fracture apertures were expanded to some extent, while some hard particles were dissolved. Additionally, the high-magnification SEM images showed that numerous microfractures occurred near organic matter (Fig. 6(h)). A thorough inspection of fine microimages showed that 82.7% of the total number of examined microfractures were unfilled (Fig. 6(a) and (c)–(h)), while a few were filled with pelite (Fig. 6(b)), calcite, or quartz, accounting for 17.3%.

Contrastingly, abnormally high-pressure fractures exhibited distinct characteristics of being filled, as evident from the thin section photographs (Fig. 6(i)). These fractures were commonly filled with quartz and calcite cements (Zhang et al., 2018; Gou et al., 2019; Lai et al., 2022; Zeng et al., 2022); thus, they were not considered to contribute to the movement of hydrocarbons and were excluded from the statistics in this study.

4.2. Interpretation of bedding-parallel fractures from FMI images

4.2.1. FMI images

FMI images contain abundant, fine geological information and are extensively employed to detect and assess fractures, structures, texture characteristics, and sedimentary beddings (Rajabi et al., 2010; Basa et al., 2019; Ezati et al., 2019; Zhang et al., 2020; Lai et al., 2022; Pang et al., 2022). Several prominent geological variables, such as bedding-parallel fractures, tectonic fractures, induced fractures, and stylolite, were identified with FMI dynamic imaging in this study (Fig. 7). Fracture evaluation focused on the dip angle, strike (Fig. 10), and developmental degree (Eqs. (1)–(6)).

The morphology of bedding-parallel fractures was observed on the FMI dynamic images as sinusoidal waves of low grayscale pixels (i.e., black and near black), with troughs and amplitudes denoting the dip direction and the size of the dip angle, respectively (Serra, 1989; Zhang et al., 2020; Lai et al., 2022). The lower the dip angle, the weaker the amplitudes; the dip angle of bedding-parallel fractures is nearly equal to that of sedimentary bedding planes, as the bedding-parallel fractures usually extend along bedding planes (Xu et al., 2020; Lai et al., 2022; Pang et al., 2022). The bedding-parallel fractures characterized with lower dip angles (<10°) were represented on at least three pads of a logging tool, with the

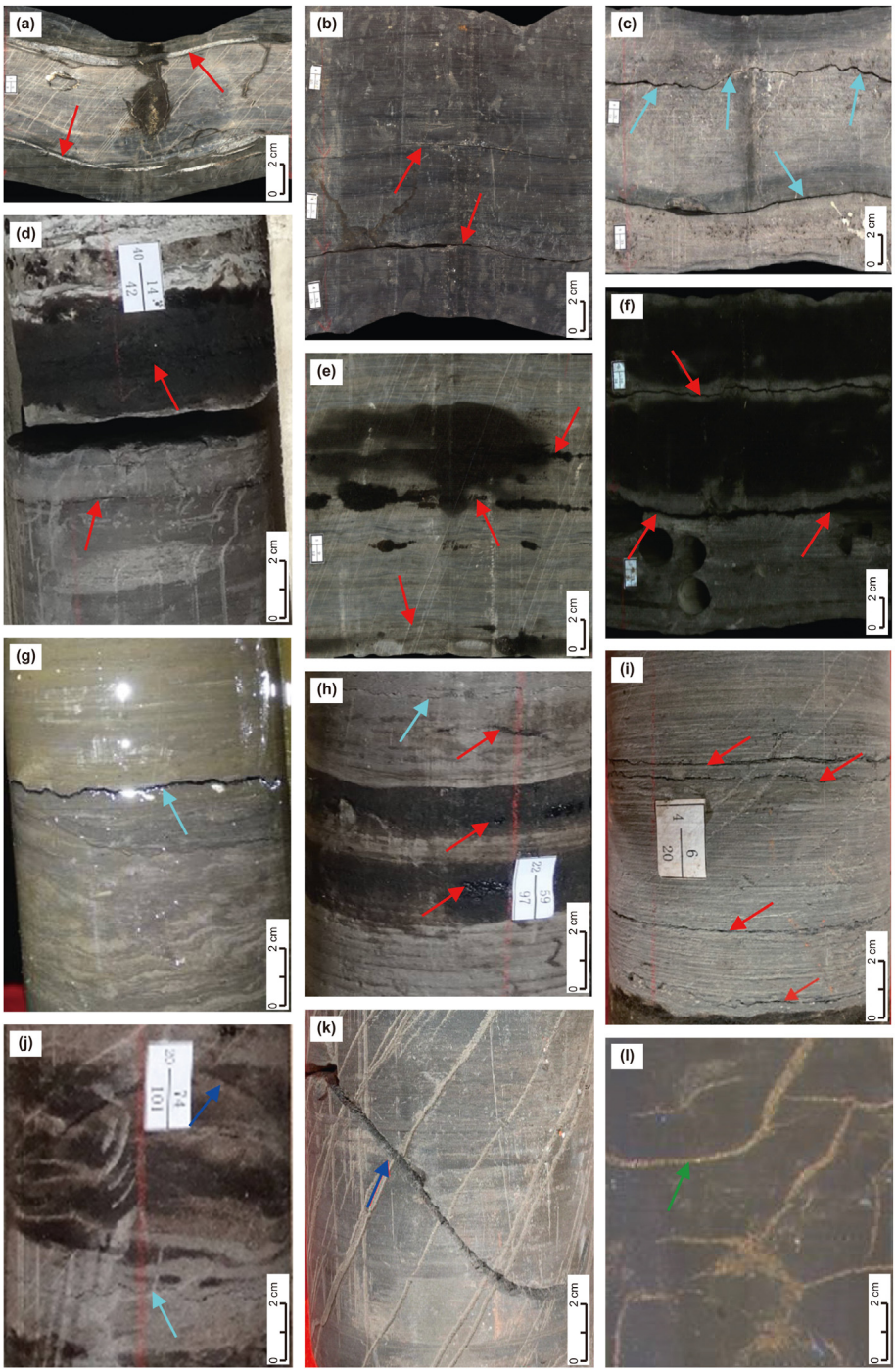

Fig. 5. Core photos showing the differences in various natural fractures in the Lucaogou Formation, Jimusar Sag. **(a)** Two bedding-parallel fractures filled by calcite (Well J29, 2311.8 m). **(b)** Unfilled bedding-parallel fractures with variable width (Well J174, 3114.1 m). **(c)** Stylolites filled by fine-grained sediments containing organic matter (Well 174, 3124.6 m). **(d)** Seeping oil along unfilled bedding-parallel fracture (Well J10025, 3796.1 m). **(e)** Dissolution and seeping oil along three distinct unfilled bedding-parallel fractures (Well J172, 2929.9 m). **(f)** Fractures parallel to bedding planes characterized by variation in width and gradual pinchout to the other end (Well 176, 3036.2 m). **(g)** Styloities filled by fine-grained sediments containing organic matter (Well J10025, 3683.8 m). **(h)** Dissolution, cementation, and seeping oil along the bedding-parallel fractures (Well J10025, 3622.8 m). **(i)** Four distinctive bedding-parallel fractures with parallel bedding surfaces (Well J10012, 3294.3 m). **(j)** A distinct high angel tectonic fracture filled mudstone and a stylolite (Well J10025, 3587.8 m). **(k)** A distinct unfilled high angel tectonic fracture (Well J10025, 3594.8 m). **(l)** Abnormal pressure fracture (Well J174, 3253.1 m).

individual fracture trace length being approximately equal to the width of the borehole image across a given window height (Zhang et al., 2020). The apertures of bedding-parallel fractures were <100 μm (Gou et al., 2019); thus, they were significantly thinner than the mudstone bands, which indicated that black or nearly black strips on FMI images are not bedding-parallel fractures (Fig. 7(a)–7(c)). Therefore, bedding-parallel fractures were well-represented by both dynamic and static images, picked put as a red sinusoidal line in this study (Fig. 7(a)–7(c)).

Tectonic fractures could be classified as conductive and resistive fractures, which are characterized by a specific dip angle (Basa et al., 2019; Zhang et al., 2020; Nian et al., 2022), as well as mixtures and often intersect sedimentary bedding surfaces (Fig. 7(c) and (d)). In the FMI images, the morphology of tectonic fractures appears

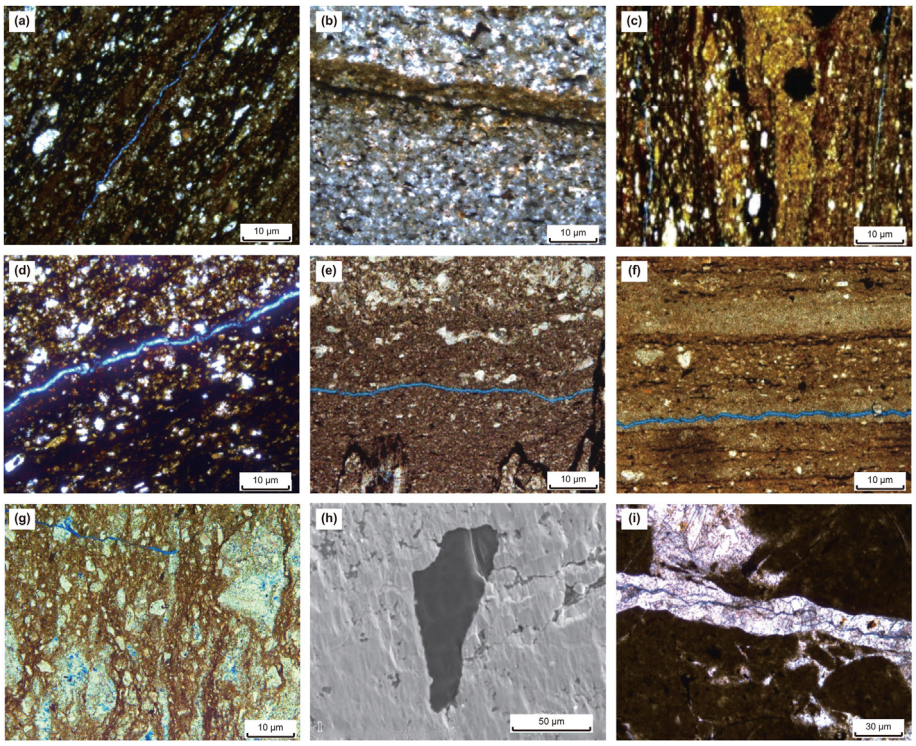

Fig. 6. Thin section and SEM images showing the bedding-parallel fractures in the Lucaogou Formation, Jimusar Sag. **(a)** Unfilled micro-fractures paralleling the lamina bypass the harder particles (Well J32, 3725.1 m). **(b)** Micro-fractures filled by mud with widths of 1–50 μm (Well J31, 2730.1 m). **(c)** Half-filled micro-fractures parallel to the lamina bypass the harder particles (Well J251, 3769.1 m). **(d)** Unfilled micro-fractures bypass the harder particles (Well J251, 3769.4 m). **(e)** Unfilled micro-fractures parallel to the lamina (Well J251, 3606.5 m). **(f)** Unfilled micro-fractures parallel to lamina (Well J31, 2859.3 m). **(g)** Structural micro-fractures and dissolution in particles (Well J174, 3272.6 m). **(h)** Micro-fractures distributed at the edge of organic matter (Well J37, 2853.8 m). **(i)** Abnormal pressure fractures filled by calcite (Well J251, 3966.6 m).

similar to that of the bedding-parallel fractures (Lai et al., 2017). When fractures are filled with low-resistivity materials (e.g., drilling mud), the morphology is shown by a sinusoidal line of low grayscale pixels, indicating conductive fractures, or high grayscale pixels, indicating resistive fractures (Zhang et al., 2020; Lai et al., 2017, 2022). In this study, conductive and resistive fractures are displayed as blue (Fig. 7(c)) and yellow (Fig. 7(d)) sinusoidal lines, respectively.

In addition to bedding-parallel fractures and natural fractures, drilling-induced fractures are also common in the Lucaogou Formation (Zhang et al., 2018; Pang et al., 2022; Zeng et al., 2022), which are usually conductive owing to the invasion of drilling mud (Tadayoni et al., 2020; Zhang et al., 2020; Lai et al., 2022). They are observed as continuous feathers or echelons of low grayscale pixels, paired, and oriented at 180° from each other (Fig. 7(e)). The direction of the drilling-induced fractures was found to be consistent with that of the current maximum principal stress (Wilson et al., 2013; Zhang et al., 2020; Nian et al., 2022).

Furthermore, borehole wall breakouts also occurred in fine-grained sedimentary rocks (e.g., shale) (Lai et al., 2022; Pang et al., 2022), as evidenced by the presence of two black or near black bands spaced at 180° in FMI images (Fig. 7(f)). In practice, borehole wall breakouts and drilling-induced fractures do not occur in the same interval simultaneously and are used to comprehensively determine the current maximum principal stress (Ezati et al., 2019; Lai et al., 2022; Pang et al., 2022).

4.2.2. Criteria for identifying bedding-parallel fractures on FMI images

In this study, the morphology of all types of fractures was represented with linear features (Ezati et al., 2019; Lai et al., 2022; Nian et al., 2022; Pang et al., 2022). The images showing a black or near black sinusoidal curve indicate that the fracture was filled with conductive materials (e.g., drilling mud) (Figs. 7(a), 7(b), 8, and 9); otherwise, the sinusoidal curves are white or bright (Fig. 7d and e). Furthermore, structural factures are mainly conductive fractures, with medium-high dip angles (Zhang et al., 2018; Zeng et al., 2022) and sharp fracture edges in the FMI images, and can cross various sedimentary beddings (Fig. 8). Compared to that of tectonic fractures, the dip angle of bedding-parallel fractures is similar to that of strata (Lu et al., 2021; Lai et al., 2022; Pang et al., 2022). Dissolution often occurs along the bedding planes in late-stage diagenetic modification, resulting in rougher fracture planes than those of tectonic fractures (Poppelreiter et al., 2010; Zhang et al., 2018; Tadayoni et al., 2020; Zeng et al., 2022). These are distinguished in the FMI images by the presence of frequent discontinuous black or near black linear characteristics (Figs. 7(a), 8 and 9) (Lai et al., 2022).

To adequately identify bedding-parallel fractures, it is necessary to distinguish them from sedimentary beddings and lithological interfaces (Poppelreiter et al., 2010; Tadayoni et al., 2020; Zhang et al., 2020). The major difference between them is that bedding-parallel fractures often show gradual thinning in the static FMI images (Fig. 9), whereas the thickness of sedimentary beddings is generally fixed, with grayscale values above the lithological interface clearly differentiated from those below it (Figs. 8 and 9).

The criteria for identifying bedding-parallel fractures in the FMI images were as follows: (1) The bedding-parallel fractures showed regularly continuous sinusoidal black or nearly black curves. (2) The sinusoidal curves extended along sedimentary bedding planes. (3) The amplitude of the sinusoidal curve was low. (4) The aperture of the sinusoidal curve was narrow (<100 μm). (5) The sinusoidal curve showed gradual thinning in the static images.

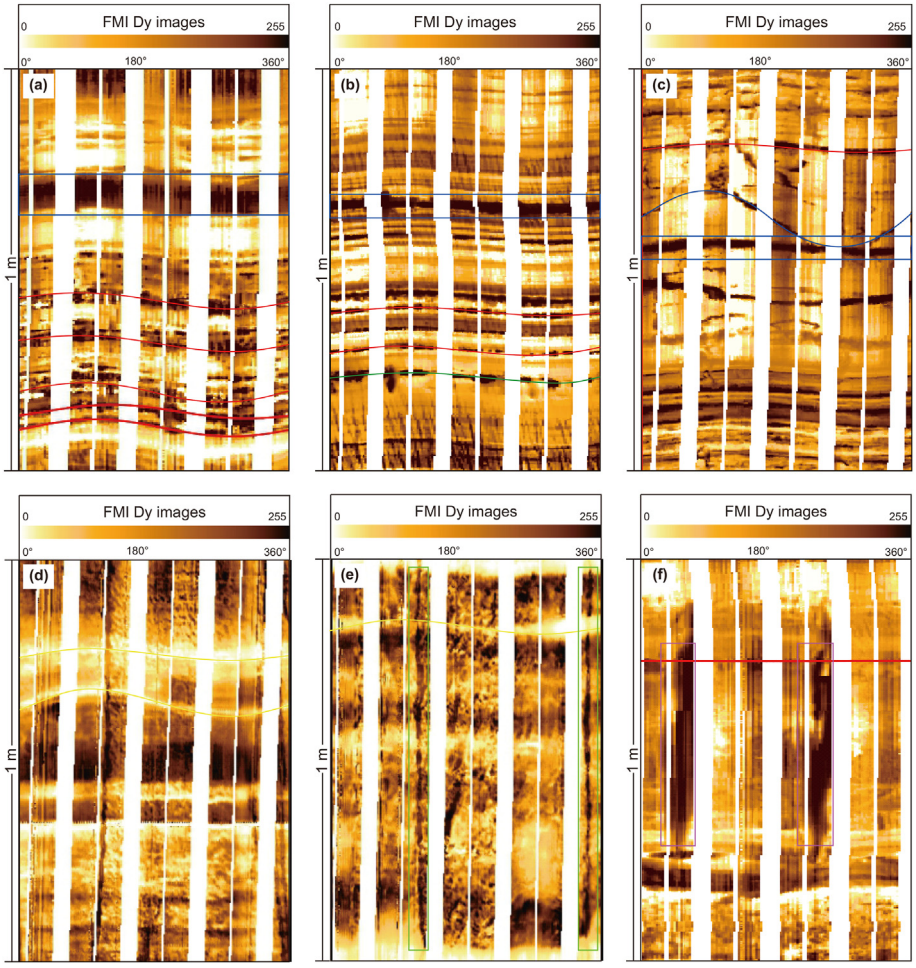

Fig. 7. Capturing geological objects with FMI dynamic images. **(a)** Bedding-parallel fractures and mudstone strip identified as red sinusoidal curves and blue region, respectively. **(b)** Stylolite identified as a green sinusoidal curve. **(c)** Conductive tectonic fractures identified as blue sinusoidal curves. **(d)** Resistive tectonic fractures identified as yellow sinusoidal curves. **(e)** Vertical conductive tectonic fractures identified as green regions. **(f)** Borehole breakouts identified as pink regions.

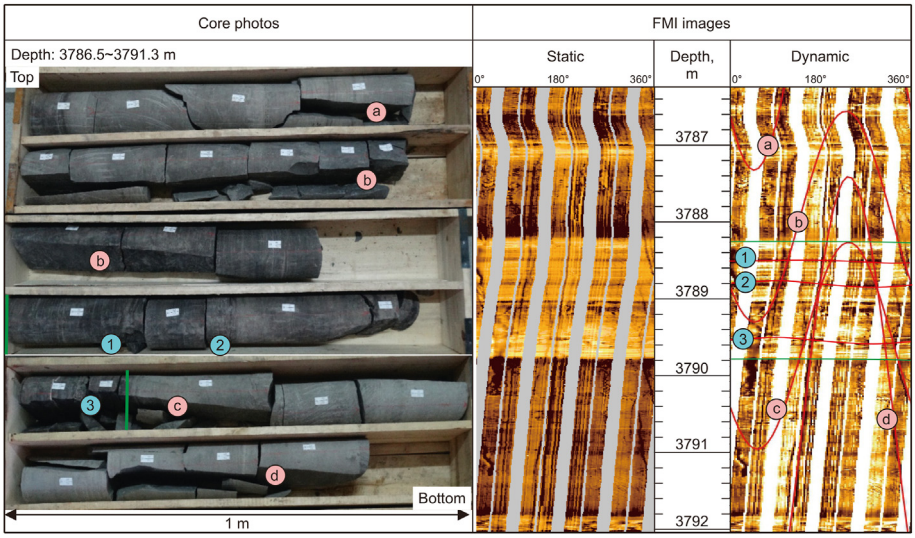

Fig. 8. Fractures in fine-grained sedimentary rocks interpreted from core photos and FMI images at 3786.5–3791.3 m in the J10025 well. Here, a, b, c, and d represent four distinct high angle conductive tectonic fractures; 1, 2, and 3 represent three unfilled bedding-parallel fractures; two green lines represent lithological interface.

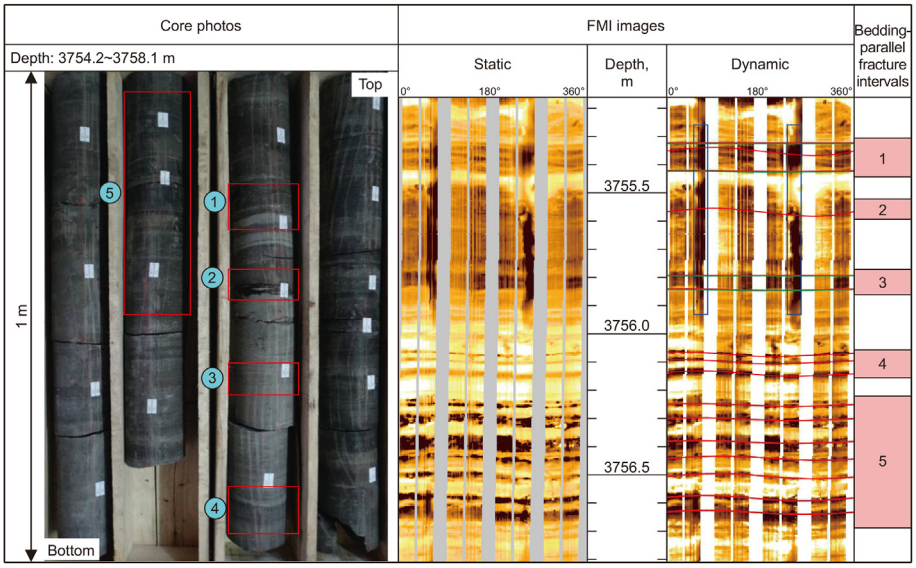

Fig. 9. Interpretation of bedding-parallel fracture intervals based on FMI images at 3754.2–3758.1 m in the J10025 well. Here, red sinusoidal waves represent bedding-parallel fractures; four green lines represent lithological interfaces; two blue regions represent borehole breakouts; 1, 2, 3, 4, and 5 and the five red regions represent five bedding-parallel fractures intervals.

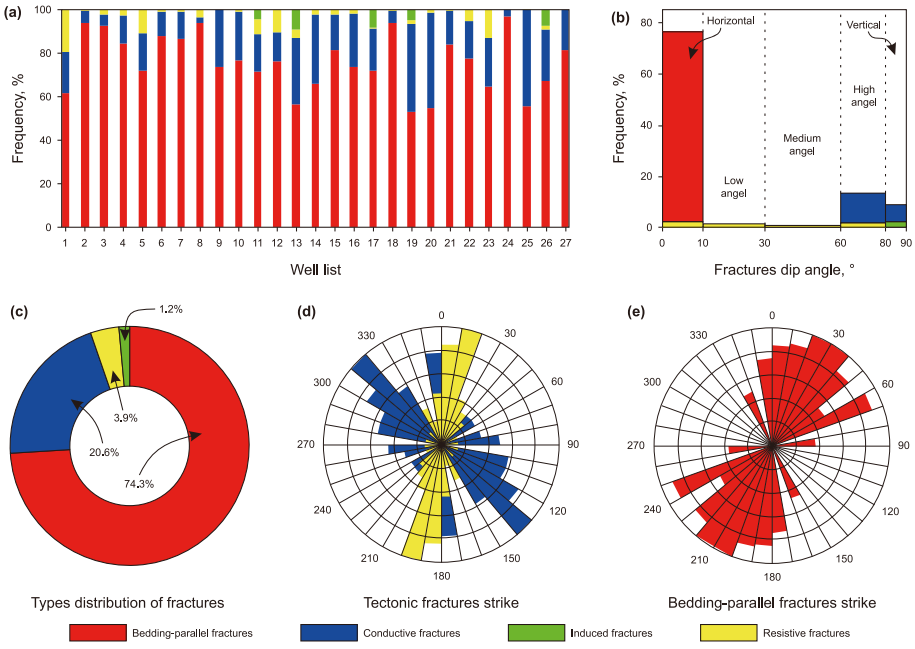

Fig. 10. Fracture occurrence and development characteristics in the Lucaogou Formation. **(a)** The distribution of different types of fractures in 27 wells indicates that the bedding-parallel fractures are most developed, followed by conductive fractures. **(b)** Fracture dip angle is primarily distributed between 0 and 10°, i.e., horizontal bedding-parallel fractures. **(c)** Doughnut chart shows the types of distribution of fractures interpreted from FMI images in the order from more to less, as follows: bedding-parallel fractures, conductive fractures, resistive fractures, and induced fractures. **(d)** Conductive and resistive fracture strikes were concentrated along the NW-SE and nearly N-S directions, respectively. **(e)** Bedding-parallel fracture strikes were concentrated along the NE-SW direction.

4.2.3. Occurrence of bedding-parallel fractures

The dip angle, strike, and inclination were used to quantitatively describe the occurrence of fractures using tadpole diagrams based on the FMI images (Gale et al., 2014; Lai et al., 2017, 2022; Zhang et al., 2020, 2022; Nian et al., 2022). Fractures were then picked based on the FMI data processed with the CIFLog software (Figs. 7-9). The apertures of bedding-parallel fractures were derived from the core observations from five coring wells. Due to the release of confining pressure during sample collection, the apparent aperture of the fractures is noticeably greater than the true aperture of fractures in the underground environment. Thus, the apparent fracture aperture observed in the cores from different lithologies was converted into the true aperture of fractures in the underground environment using the amending formula proposed by Lu et al. (2021). Statistics showed that the aperture values of bedding-parallel fractures in dolomite (including silty dolomite), muddy siltstone, and dolomitic siltstone were in the ranges of 10–100 μm (an average of 37 μm), 10–60 μm (an average of 31 μm),

and 10–90 μm (an average of 35 μm), respectively.

In this study, the following four types of fractures were recognized in the FMI images of 27 wells according to the proposed identification criteria: resistivity fractures (3.9%), conductive fractures (20.6%), bedding-parallel fractures (74.3%), and induced fractures (1.2%) (Fig. 10(a) and (c)). Among these, horizontal fractures were the most common, accounting for 76.4% of the total number of fractures, while high angle and vertical fractures accounted for 13.3% and 8.8%, respectively (Fig. 10(b)).

The tectonic fracture statistics for various fill materials revealed that the strike of conductive fractures had a predominantly NW-SE direction (Fig. 10(d)), which is in accordance with the orientation of the present maximum principal stress (Lyu et al., 2017; Zhang et al., 2018; Tadayoni et al., 2020; Zeng et al., 2022). These resistive fracture strikes were primarily concentrated in the N-S direction (Fig. 10(d)), which is strongly in agreement with the orientation of the maximum principal stress in the Hercynian period (i.e., N-S compressional stress) (Liu et al., 2017; Kuang et al., 2019; Zhang et al., 2018). This suggests that the resistive fractures are intimately related to the Late Hercynian tectonic activity.

Compared to that of tectonic fractures, the development of bedding-parallel fractures was found to be considerably affected by diagenesis modification, hydrocarbon generation, and acid expulsion, whereas the influence of tectonic activities was weak (Liu et al., 2017; Zhang et al., 2018; Lin et al., 2021; Zeng et al., 2022). These results indicate that the occurrence of bedding-parallel fractures is closely related to that of strata and is characterized in a highly consistent manner (Liu et al., 2020; Lai et al., 2022; Pang et al., 2022). The Lucaogou Formation was deposited during the Hercynian period (Kuang et al., 2019; Tong et al., 2018; Wang et al., 2020). Although it was influenced by several post-depositional tectonic activities in the Indosinian, Yanshanian, and Himalayan stages, these were weak and did not substantially transform the stratigraphic strike. Hence, the bedding-parallel fracture strike was approximately consistent with that of the resistivity fractures in the Hercynian period, which showed a predominately NE-SE direction (Fig. 10e) (Zhang et al., 2018; Lai et al., 2022).

4.3. Quantitative parameters for characterizing the development of bedding-parallel fractures in fine-grained sedimentary rocks

Several quantitative parameters were established using the FMI images and conventional curves to characterize the development of bedding-parallel fractures (~mm), and corresponding maps were produced to establish the characterization methods (Fig. 11). The quantitative parameters for characterizing the bedding-parallel fractures were as follows: the single reservoir interval, reservoir interval density of bedding-parallel fractures, weighted matrix porosity of reservoir interval, matched matrix porosity of sweet spot interval, and matched sweet spot density of bedding-parallel fractures.

4.3.1. Single reservoir interval

Single reservoir intervals consisted of continuous oil layers (identical or diverse types) in the longitudinal direction (Fig. 3) (Aghli et al., 2016; Pang et al., 2022; Zhang et al., 2022). Based on the calibration of logging datasets with core samples and thin section photographs, the conventional log values and morphological combination (primarily GR, DEN, AC, CNL, RT, and RI) were integrated, and the oil layer was interpreted for each point with the petrophysical model using the CIFLog software. For characterizing the development of bedding-parallel fractures, the thickness of each oil layer should be more than 0.5 m (Zhang et al., 2022). Using well J10025 as an example, the matrix porosity, oil saturation, oil layer, and reservoir interval were obtained and are presented in Fig. 11.

4.3.2. Reservoir interval density of the bedding-parallel fractures

Fracture density, commonly referred to as the fracture linear density, indicates the extent to which countable fractures (e.g., oblique fracture, bedding-parallel fractures) develop based on the thickness in the FMI images (Lai et al., 2017; Lu et al., 2021; Zhang et al., 2022). While invisible microfractures and mesh fractures that are actually present cannot be considered, they occur in association with countable fractures (Shi and Qiu, 2021; Lai et al., 2022). In a single reservoir interval, the presence of many countable fractures indicates a high development capacity. To characterize the development capacity of all fractures in a reservoir interval, the BFd_{RI} was calculated (Fig. 3). For fine-grained sedimentary rocks, it was found that the reservoir interval density of bedding-parallel fractures was not only suitable for selecting reservoirs during perforation development but was also a mesoscale fracture parameter for predicting fractures using 3D seismic data (Dong et al., 2022; Bao et al., 2023). Fig. 11 shows that the 3558.6–3561.7 m interval is a reservoir interval for a total of nine bedding-parallel fractures. Thus, the reservoir interval density of bedding-parallel fractures was 2.9 m^{-1}.

4.3.3. Weighted matrix porosity of the reservoir interval

The weighted matrix porosity of the reservoir interval (ϕ_{RI}) represented the mathematical statistic matrix porosity of a single reservoir interval comprising multi-continuous oil layers (Fig. 3). Compared with the average matrix porosity, the weighted matrix porosity emphasizes the contribution of the thick oil layer to matrix porosity and is more widely applied in geological research and for calibrating seismic attributes. Fig. 11 shows that the 3540.6–3544.7 m interval is a reservoir interval consisting of four oil layers in the J10025 well. Here, the statistical weighted matrix porosity was 18.2% and the average matrix porosity was 17.8%.

4.3.4. Matched porosity of sweet spot intervals

The matched matrix porosity of sweet spot intervals was used to characterize the porosity of longitudinal reservoir assemblies (Fig. 3). The reservoir assemblies (i.e., sweet spots) can be identified based on sensitive seismic attributes (Savin et al., 2005; Dong et al., 2022; Bao et al., 2023). Here, a cross plot between logging porosity and seismic attributes for a sweet spot section was established, and a specific functional relationship between the two was established (Li et al., 2018). The identical scale porosity was used to validate the interwell matrix porosity model and predict bedding-parallel fractures using 3D seismic data.

4.3.5. Matched sweet spot density of bedding-parallel fractures

The matched sweet spot density of bedding-parallel fractures ($MBFd_s$) can also be considered as a macroscale fracture parameter, providing a meaningful link to transform data scales between logging parameters and seismic attributes (Fig. 3). Fig. 11 shows that the 3552.4–3564.3 m interval is a sweet spot interval corresponding to 3D seismic data and includes four reservoir intervals. In this case, the matched sweet spot density of the bedding-parallel fractures was calculated considering the four reservoir interval densities of bedding-parallel fractures, while the weighting coefficients were considered as the weighted matrix porosity of the reservoir interval.

4.4. Characterization of the distribution of bedding-parallel fractures

A practical application was performed to assess the extent to which the proposed model could accurately predict the

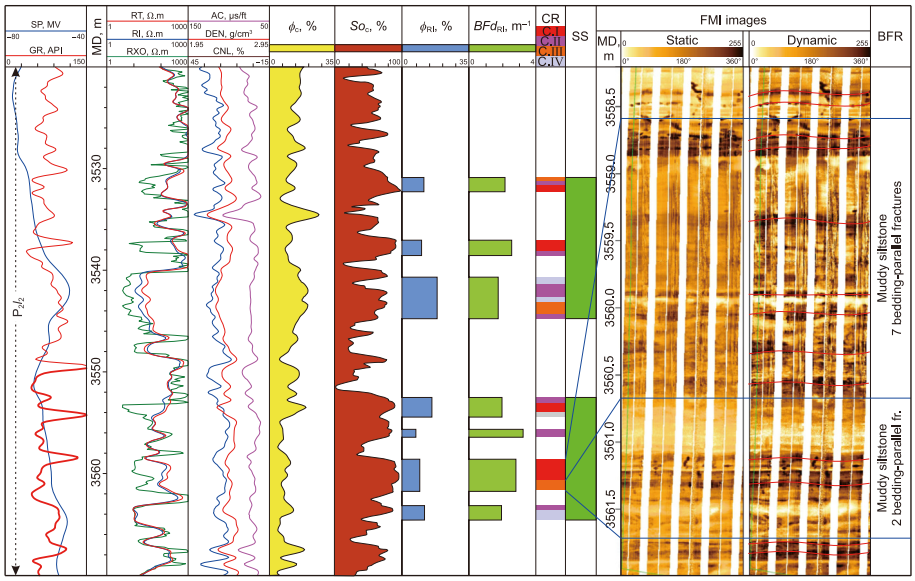

Fig. 11. Interpretation of matrix porosity, oil saturation, and bedding-parallel fractures based on conventional well logs and FMI images from the J10025 well. ϕ_c and So_c: Calculated porosity and oil saturation from conventional well logs, respectively. ϕ_{RI}: Weighted matrix porosity of a reservoir interval. BFd_{RI}: Reservoir interval density of bedding-parallel fractures. CR: Results from conventional well logs. C.I: Class I oil layer. C.II: Class II oil layer. C.III: Class III oil layer. C.IV: Class IV oil layer. SS: Sweet spot interval. BFR: Interpreted results of bedding-parallel fractures from FMI images.

development of bedding-parallel fractures based using seismic attributes. Figs. 11 and 14 show the relevant results to describe bedding-parallel fracture development.

4.4.1. Longitudinal distribution of bedding-parallel fractures in a single well

The method was tested in well J10025 in the Jimusar Sag. The evaluation results of bedding-parallel fractures from seven reservoir intervals are displayed in Fig. 11. The low-resistivity intervals were closely related to the bedding-parallel fractures, as evidenced by their development in the single well (Fig. 11). Bedding-parallel fractures did not usually appear in high-resistivity intervals. On the contrary, several bedding-parallel fractures can be identified in the yellow-dark intervals on the FMI images (Zhang et al., 2020; Lai et al., 2022; Pang et al., 2022). This is especially evident at the interbedded brittle, which corresponds to the intermittent dark/light strips on the FMI images and has more bedding-parallel fractures (Figs. 7 and 9). This indicates that the logging resistivity curve can indicate the approximate developmental position of bedding-parallel fractures in the longitudinal direction (Lai et al., 2022), but it cannot characterize the intensity of development of bedding-parallel fractures.

Fortunately, the logging interpretation matrix porosity seemed to be well correlated with the development of bedding-parallel fracture (Fig. 11). Our analyses revealed that the BFd_{RI} and weighted matrix porosity of the reservoir interval (ϕ_{RI}) were closely correlated (Fig. 11). After combining the 59 interpretation datasets of 27 wells, the weighted matrix porosity of reservoir intervals (ϕ_{RI}) was fitted with BFd_{RI} (Fig. 12). The lower the ϕ_{RI}, the higher was the BFd_{RI}. These results indicate an overall negative exponential correlation between these parameters, with a multiple correlation coefficient as high as 0.7649. The specific functional expression obtained is as follows:

$$BFd_{RI} = 3.3561 \cdot e^{-0.064 \cdot \varphi_{RI}} \quad (7)$$

Moreover, in a single well, bedding-parallel fractures primarily occurred in low-resistivity intervals, which indicated that the intensity of their developmental can be predicted from the weighted matrix porosity of the reservoir interval.

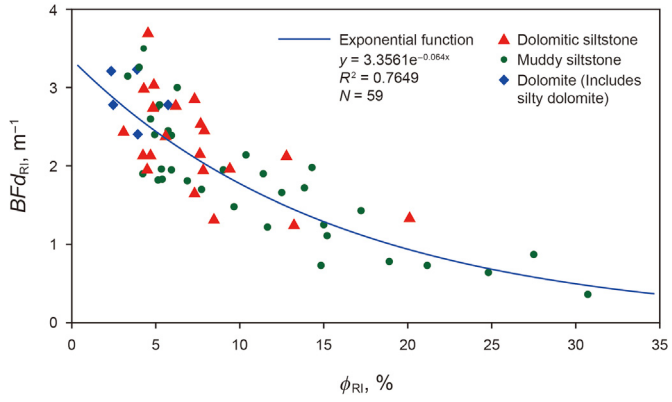

Fig. 12. Gradual decrease in the reservoir interval density of bedding-parallel fractures for each of the three major lithological fine-grained sedimentary rocks with increasing weighted matrix porosity of a reservoir interval; cross plots showing the overall better negative correlation of them. BFd_{RI}: Reservoir interval density of bedding-parallel fractures; ϕ_{RI}: Weighted matrix porosity of a reservoir interval.

4.4.2. Planar distribution of bedding-parallel fracture development

Multi-scale matching and step-by-step progressive methods were employed to predict the planar distribution of bedding-parallel fracture development. Integrated method testing was implemented in the upper sweet spot in the Lucaogou Formation (Fig. 1(b) and (d)). Based on the results interpreted from logging datasets and seismic attribute analysis, a predicted matrix porosity isogram (P-ϕ_s) for the upper sweet spot was acquired (Fig. 13), showing that matrix porosity mainly ranged from 6% to 15%.

with only a few separate values greater than 14% in the southeastern part of the study area (e.g., J22, J301, and J221 well blocks). Overall, the high matrix porosity (>15%) in the central areas extended for 15 km in the NW-SE direction, with a width of ~6 km. The isogram of the developmental intensity of bedding-parallel

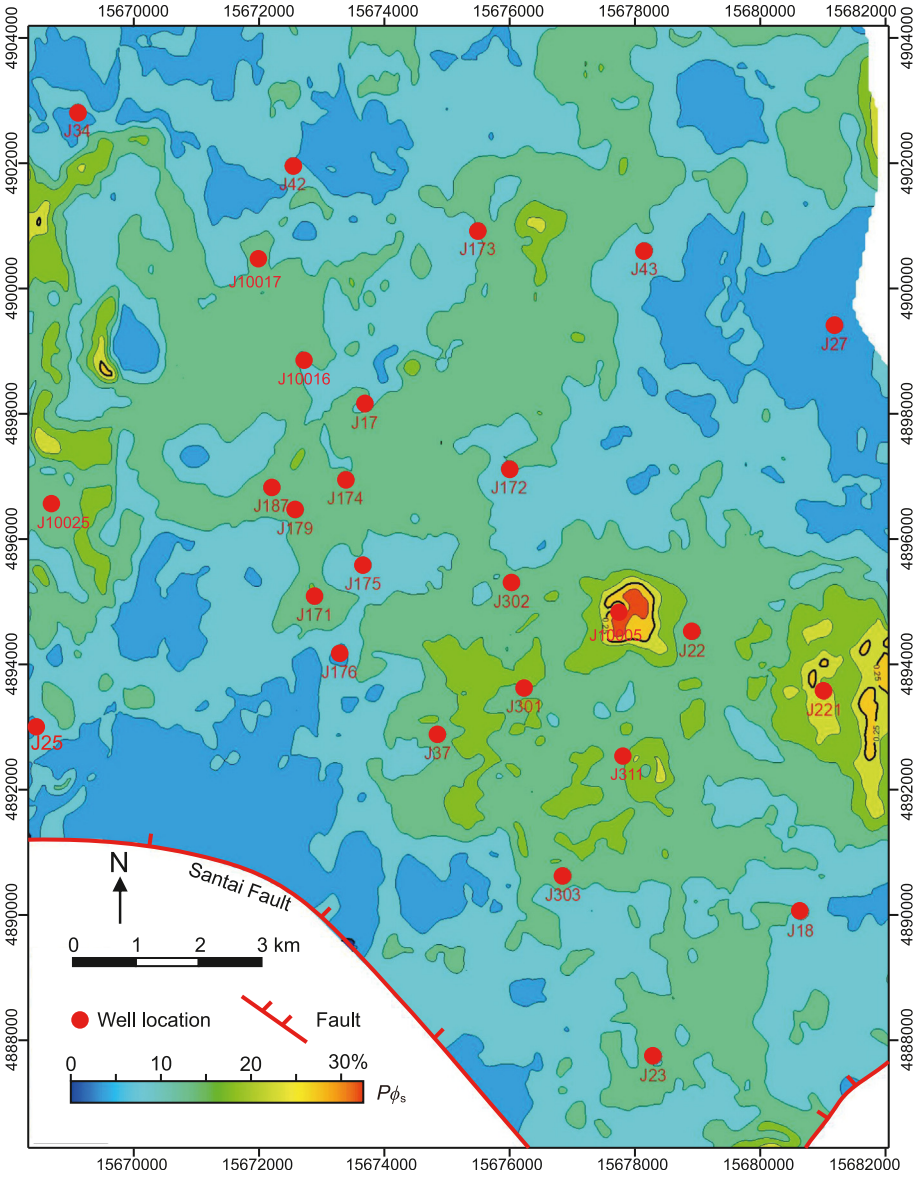

Fig. 13. Regional distribution of the predicted matrix porosity in the upper sweet spot interval ($P\phi_s$) of Lucaogou Formation, Jimusar Sag.

fractures ($PBFd_s$) was subsequently produced using the Strata software (Fig. 14). It primarily ranged from 1.25 to 2.5 m^{-1}, presenting significant heterogeneity. Simultaneously, the developmental degree of bedding-parallel fractures was weak ($PBFd_s$ < 1.5 m^{-1}) in the central areas and strong along the margin. However, certain isolated areas in the middle part of the study area (e.g., J172, J173, J175, and J10016 well blocks) showed greater values of $PBFd_s$ (> 1.75 m^{-1}).

5. Discussion

5.1. Factors affecting the development of bedding-parallel fractures

Previous studies on the formation mechanisms of bedding-parallel fractures have shown that their genesis is predominantly linked to tectonic evolution, diagenesis modification, and hydrocarbon generation in the Permian Lucaogou Formation in the Jimusar sag (Gao and Li, 2016; Ma et al., 2017; Zhang et al., 2017; Basa et al., 2019; Zeng et al., 2022). These factors, which control the development of bedding-parallel fractures, can be classified into intrinsic reservoir factors—primarily sedimentation, minerals, lithology, total organic carbon content, and thickness, and extrinsic tectonic factors, including tectonic stress and faults.

5.1.1. Intrinsic reservoir factors

Multi-complex intrinsic reservoir factors generally lead to variations in the development of bedding-parallel fractures in fine-grained sedimentary rocks, which can substantially promote or weaken each other (Cobbold et al., 2013; Zhang et al., 2017, 2021; Wu et al., 2019; Gu et al., 2020; Gasparrini et al., 2021; Lu et al., 2021; Su et al., 2022). If they are considered simultaneously, the influence of specific factors on the development of bedding-parallel fractures cannot be fully revealed. Therefore, in this study the effects of mainly intrinsic reservoir factors on the development of bedding-parallel fractures were investigated separately using statistical methods (Fig. 15).

Bedding-parallel fractures are generally assumed to originate in petrologically firmer beds and terminate at bedding surfaces

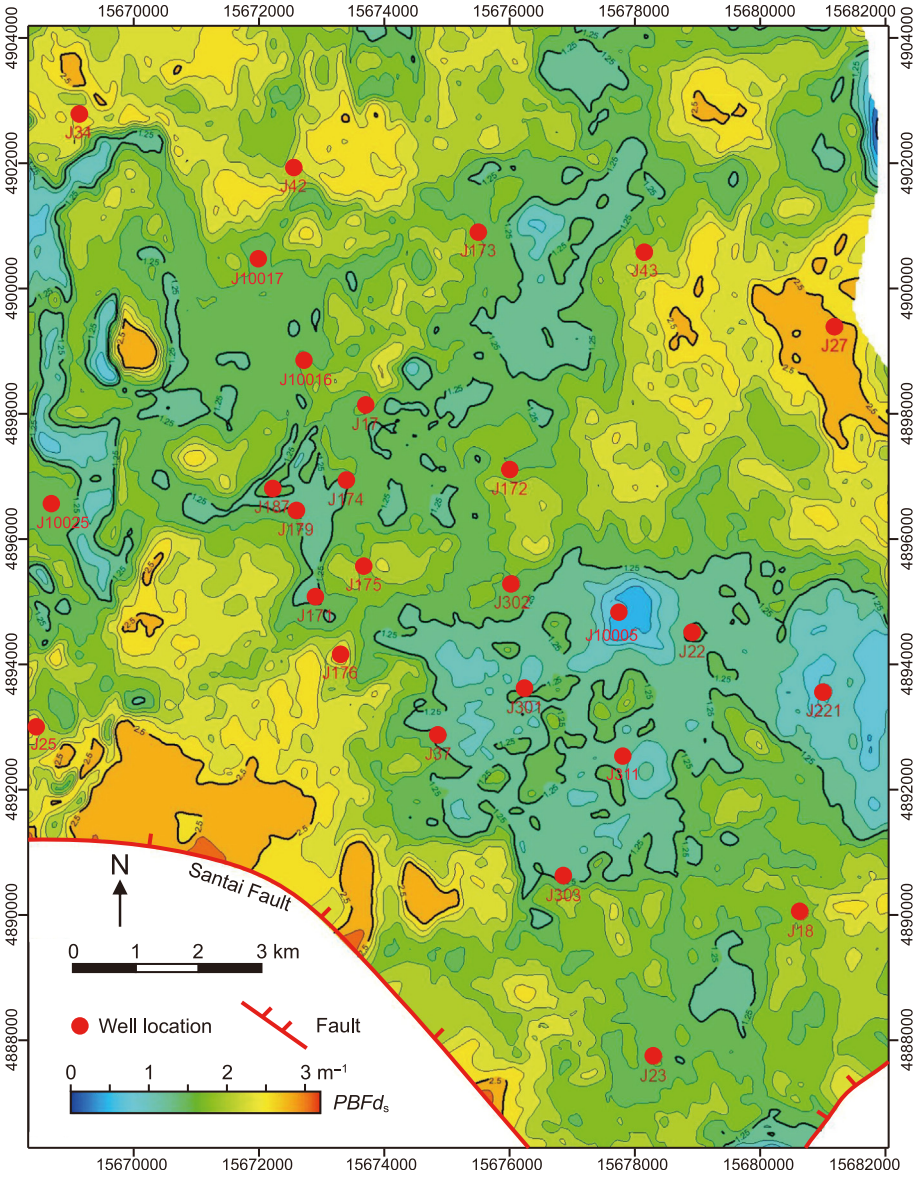

Fig. 14. Regional distribution of the predicted sweet spot density of bedding-parallel fractures ($PBFd_s$) of upper sweet spot interval in Lucaogou Formation, Jimusar Sag.

(Figs. 5(a)–5(i), 6(a)–6(f)) (Rajabi et al., 2010; Cobbold et al., 2013; Gale et al., 2014; Liang et al., 2021; Lai et al., 2022; Liu et al., 2022). Thus, variations in minerals can affect the intensity of the developmental of bedding-parallel fractures in fine-grained sedimentary rocks (Bergbauer and Pollard, 2004; Altawati et al., 2021; Xu et al., 2021; Lai et al., 2022; Xie et al., 2022). The X-ray diffraction results of 87 samples from the upper sweet spot in the Lucaogou Formation show that predominant minerals include carbonate minerals (mainly dolomite and a few calcites), quartz, feldspar (primarily plagioclase and minor K-feldspar), and clay minerals, with average contents of 38.6%, 26.3%, 22.8%, and 10.2%, respectively. The mechanical performance of several typical minerals were examined according to their elastic modulus, Poisson's ratio, and fracture toughness, revealing the following order of brittleness: dolomite > quartz > plagioclase > clay minerals (Hooker et al., 2019; Heng et al., 2020; Liang et al., 2021; Xu et al., 2021; Zeng et al., 2022). Dolomite and quartz are typical brittle minerals, characterized by high modulus of elasticity, low Poisson's ratios, and low fracture toughness, whereas clay minerals are typical plastic minerals, and feldspar has a medium brittleness. Brittle minerals (including dolomite and quartz) exert a considerable effect on the extent of the development of bedding-parallel fractures. High contents of brittle minerals indicate a high degree of the development of bedding-parallel fractures. The cross plots between the brittle mineral content and the BFd_{RI} were plotted based on the X-ray diffraction results and interpretation of logging data (Fig. 15(a)), which showed a clear monotonic relationship between them. These results indicated that the reservoir interval density of bedding-parallel fractures increased with the brittle mineral content. However, brittle mineral contents corresponding to the values of the reservoir interval density of bedding-parallel fractures showed a wide range (Fig. 15(a)), indicating that other factors also affect the development of bedding-parallel fracture.

The upper sweet spot in the Lucaogou Formation comprises muddy siltstone, dolomitic siltstone, and dolomite, which are deposited in shore-shallow lacustrine and beach-bar facies (Yang et al., 2018; Zhang et al., 2019; Zhi et al., 2019; Lin et al., 2021). These lithologies have different mineral compositions and

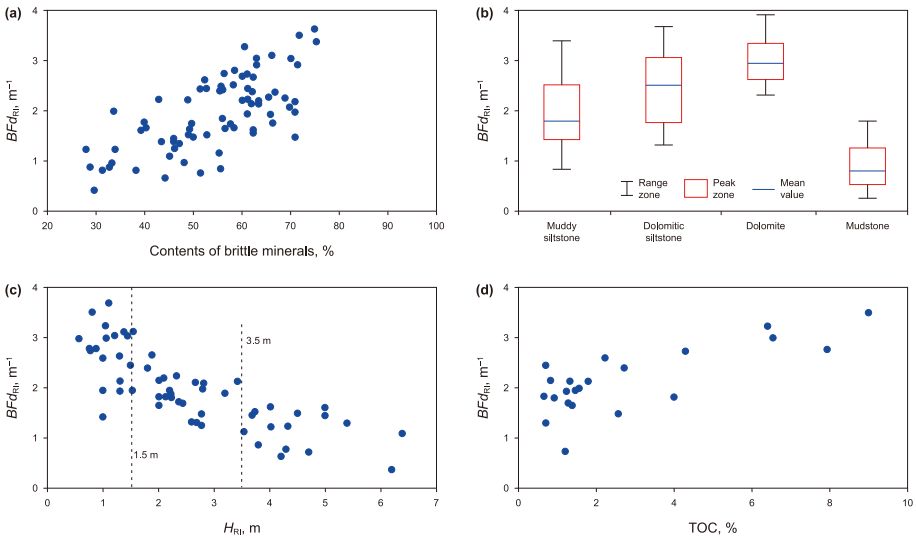

Fig. 15. Effects of intrinsic reservoir factors on the development of bedding-parallel fractures (indicate by reservoir interval density of bedding fractures). **(a)** As the contents of brittle minerals increase, the reservoir interval density of bedding-parallel fractures gradually increases. (**b**) Box diagram of the reservoir interval density of bedding-parallel fractures shows that the bedding-parallel fractures are most developed in dolomite, followed by dolomitic siltstone and muddy siltstone. **(c)** With increasing thickness of the single reservoir interval, the reservoir interval density of bedding-parallel fractures gradually decreases in the all, while poor correlation of them were found within a thickness of 1.5 m and greater a thickness of 3.5 m. **(d)** Better positive correlation between *TOC* and reservoir interval density of bedding-parallel fractures. BFd_{RI}: reservoir interval density of bedding-parallel fractures; H_{RI}: single reservoir interval accumulative thickness; *TOC*: total organic carbon contents.

abundant bedding structures (e.g., parallel, oblique, and cross beddings), which lead to distinct differences in the degree of development of the bedding-parallel fractures. The observation of core samples from five coring wells revealed that the degree of the development of bedding-parallel fractures was the most intense in dolomite reservoirs, followed by that in dolomitic siltstone and muddy siltstone reservoirs. The logging data of the reservoir interval density of bedding-parallel fractures also showed similar results (Fig. 15(b)). Based on the box diagrams for muddy siltstone, dolomitic siltstone, dolomite, and mudstone, the values of reservoir interval density of bedding-parallel fractures were 1.45–2.55 m^{-1} (mean value = 1.85 m^{-1}), 1.83–3.05 m^{-1} (2.56 m^{-1}), 2.73–3.38 m^{-1} (2.98 m^{-1}), and 0.55–1.26 m^{-1} (0.81 m^{-1}), respectively. These statistical results reveal that the sequence of the developing degree of bedding-parallel fractures at different lithologies in the Lucaogou Formation is dolomite > dolomitic siltstone > muddy siltstone > mudstone. In particular, in the case of similar mineral components, finer rock particles indicate highly developed bedding-parallel fractures. Core observation results showed that the fracture development in siltstone was better than that in fine sandstone, followed by medium sandstone, and conglomerate (Figs. 8 and 9). These results indicate that the granularity of rock particles also affects the degree to which bedding-parallel fractures develop. Moreover, the heterogeneity of the reservoir interval structure (contact relationship and arrangement of minerals) also affects the development of bedding-parallel fractures (Loucks et al., 2009; McGinnis et al., 2017; Lai et al., 2022; Pang et al., 2022). Under the conditions of compression caused by the same tectonic stress, differences in the structural deformation of reservoir intervals often result in a variation in the degree of development of bedding-parallel fractures and their direction.

Apart from minerals and lithological factors, individual reservoir interval thickness is also a non-negligible intrinsic factor influencing the degree to which bedding-parallel fractures develop (Yawar and Schieber, 2017; Zhang et al., 2018; Lu et al., 2021; Zeng et al., 2022; Liu et al., 2023). Compared to the rock matrix, bedding planes are weak interfaces (Gale et al., 2014; Lin et al., 2021). In this study, bedding-parallel fractures usually occurred within the rock layer and did not intersect with the bedding planes (Figs. 7(a), 7(b), and 9). The degree to which bedding-parallel fractures developed within individual reservoir intervals was examined based on the interpretation of logging data from 27 wells. Statistical analysis showed that the reservoir interval density of bedding-parallel fractures decreased with an increase in the thickness of single reservoir intervals (Fig. 15(c)). The reservoir interval density of bedding-parallel fractures was the highest for single reservoir intervals with thickness <1.5 m while was poorly correlated on them. This can be attributed to the presence of several laminae with weak interfaces in the thinner reservoir interval, which promote the development of bedding-parallel fractures, resulting in a poor relationship between the reservoir interval density of bedding-parallel fractures and the thickness of single reservoir intervals. For single reservoir intervals thicker than 3.5 m, thickness had only mild effects on the development of bedding-parallel fractures. That is, under equal tectonic stress conditions, thinner reservoir intervals are more prone to diastrophism, resulting in stronger fracturing. The thinner reservoir intervals constrained the overall development of bedding-parallel fractures (Zhang et al., 2018, 2022; Zeng et al., 2021; Lai et al., 2022); however, the ratio of the number of bedding-parallel fractures developed within reservoir intervals to their thickness was relatively large, indicating that the reservoir interval density of bedding-parallel fractures in thinner reservoirs was larger. This is because the statistical unit used to calculate the reservoir interval density of bedding-parallel fractures was less reservoir thickness. Conversely, thicker reservoir intervals had more space for bedding-parallel fracture development and a higher total bedding-parallel fracture count than thinner reservoir intervals. However, owing to the sharp increase in reservoir thickness, the reservoir interval density of bedding-parallel fractures was relatively small. In addition, an analysis of the number of bedding-parallel fractures directly identified in FMI images in the sweet spot section from the 27 wells in the study area and the thickness of the sweet spot section indicated that as the thickness of the sweet spot section increased, the total number of bedding-parallel fractures increased overall (Fig. 16(a)), but the sweet spot density of bedding-parallel fractures gradually decreased

(Fig. 16(b)). These statistical results indicate that the thickness of fine-grained sedimentary rocks has a negative influence on the overall development of bedding-parallel fractures under the same mineral composition, tectonic stress, temperature, and geofluid conditions.

Effective source rocks of the Lucaogou Formation in Jimusar Sag are widely distributed and mainly comprise mudstone, shale, silty mudstone, dolomitic mudstone, and calcareous mudstone (Zhang et al., 2019; Lu et al., 2021; Pang et al., 2022). The total organic carbon content (TOC) of source rocks was primarily 0.68–9.13%, with an average of 3.58%. Under nearly equal tectonic stress, TOC may also affect the development of bedding-parallel fractures due to hydrocarbon generation (Xiang et al., 2013; Kuang et al., 2015; Zhang et al., 2018, 2021; Wu et al., 2019; Wang et al., 2021; Zeng et al., 2021, 2022), which was considerably reflected by the distribution of organic matter. The higher the TOC, the greater the extent of the development of bedding-parallel fractures in the middle or along the margin of the organic matter strips is expected to be. This phenomenon was frequently observed in the SEM images (Fig. 6(h)). To visualize the relationship between TOC and the reservoir interval density of bedding-parallel fractures, the average TOC near the reservoir interval and corresponding reservoir interval density of the bedding-parallel fractures were selected, and their cross plots were drawn (Fig. 15(d)). Results showed that the reservoir interval density of bedding-parallel fractures increased with increasing TOC, indicating that an increase in TOC promotes the development of bedding-parallel fractures to some extent.

5.1.2. Extrinsic tectonic factors

In contrast to the intrinsic reservoir factors that control bedding-parallel fracture development at the millimeter-/centimeter-scale, extrinsic tectonic factors mainly affect the distribution at the meter-/kilometer-scale (Zhang et al., 2018; Heng et al., 2020; Xu et al., 2020; Dong et al., 2022; Liu et al., 2022; Su et al., 2022; Zeng et al., 2022). Most fractures mainly occurred at areas with released tectonic stress, such as fault belts, fault transformation zones, sub-fault development areas, and the top of local structures (Zhang et al., 2022). Therefore, the macroscale distribution of bedding-parallel fractures was related to the tectonic evolution of the study area. The Jimusar Sag is far away from the structural belts of Junggar Basin (Fig. 1(b)). Thus, its strata have mainly experienced overall uplift or settlement without largescale deformation or displacement (Qiu et al., 2016; Kuang et al., 2019; Wu et al., 2019), resulting in undeveloped tectonic fractures. Nevertheless, the magnitude and direction of paleotectonic stress considerably varied among different tectonic activity periods (Zhang et al., 2018; Heng et al., 2020; Su et al., 2022; Zeng et al., 2022). The tectonic compression is expected to significantly promote the development of bedding-parallel fractures and the unsealing nature. As strata compressed by tectonic stress have weak bedding planes that are mechanically prone to fracture, bedding-parallel fractures develop.

Fig. 1(b) shows the Santai fault and its branch faults to the southwest and south of the Jimusar Sag as well as two sub-faults to the east. The strata of the Lucaogou Formation in the northern edge of the study area are steeper, especially the J29 and J34 well blocks. These specific geological structures affect the overall development of bedding-parallel fractures. Fig. 14 shows the planar distribution of the predicted sweet spot density of bedding-parallel fractures ($PBFd_s$), which have a banded distribution. The analysis of matched sweet spot density of bedding-parallel fractures showed that the average values near the mentioned specific geological structures and other areas were 2.37 m^{-1} and 1.21 m^{-1}, respectively. In other words, the degree to which bedding-parallel fractures developed was consistent with the distribution of these specific geological structures (McGinnis et al., 2017; Zhang et al., 2018; Wei et al., 2021; Su et al., 2022; Zeng et al., 2022). Moreover, as the distance between these specific geological structures increased, the degree of the development of bedding-parallel fractures gradually decreased.

In conclusion, both the intrinsic reservoir conditions and extrinsic tectonism affect the development of bedding-parallel fractures in the Lucaogou Formation. While the intrinsic reservoir factors are a prerequisite for the development of bedding-parallel fractures, the extrinsic tectonic factors substantially promote their development. Under similar or the same reservoir intervals, the degree of development of bedding-parallel fractures located in the fault belts or at the top of local structures is considerably higher than that of fractures located in other areas. Contrastingly, under the same structural conditions of the reservoir intervals, the intrinsic reservoir factors play a major role in the development of bedding-parallel fractures.

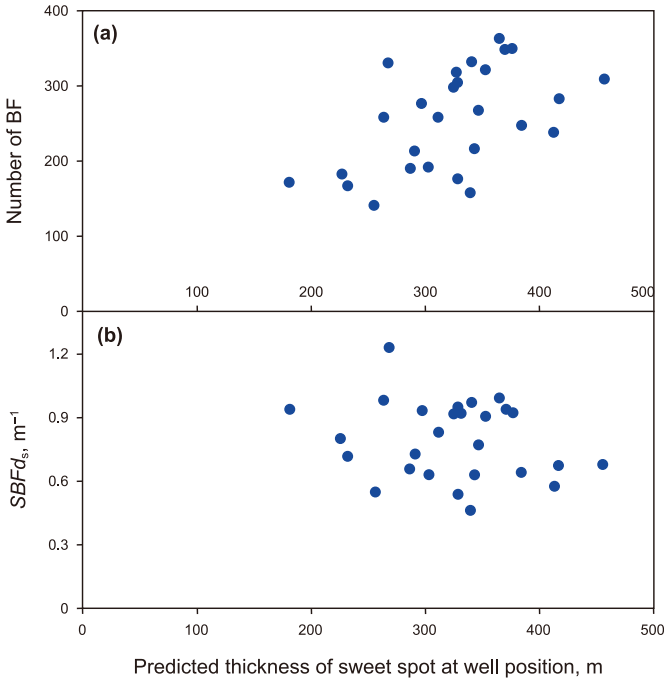

Fig. 16. Statistical relationships between the degree of the development of bedding-parallel fractures and the thickness of the predicted sweet spot. As the thickness of the sweet spot increases, the number of bedding-parallel fractures gradually increases **(a)**, and the statistical sweet spot density of bedding-parallel fractures ($SBFd_s$) on the opposite **(b)**.

5.2. Relationship between bedding-parallel fracture development and the physical properties of reservoirs

Bedding-parallel fractures extensively occurred in the fine-grained sedimentary reservoirs of the Lucaogou Formation in the Jimusar Sag, and presented heterogeneity in the single well and planar distribution (Figs. 11 and 14). The variation in the development of bedding-parallel fractures is responsible for the differing physical properties and petroleum-bearing capacity (Liu et al., 2017; Lu et al., 2021). We investigated the effects of bedding-parallel fracture development on the physical properties and petroleum-bearing capacity of reservoirs by considering the proposed parameters for the characterizing the development of bedding-parallel fractures, i.e., the BFd_{RI}. To simplify the comparison, all samples were classified into two groups, with and without bedding-parallel fractures, and diagrams of the reservoir interval density of bedding-parallel fractures vs. matrix porosity,

permeability, and oil-bearing properties were drawn (Figs. 2 and 16).

The simultaneous presence of diverse pores and bedding-parallel fractures in the Lucaogou Formation adds complexity to its fracture network (Kuang et al., 2015; Yang et al., 2018; Zhang et al., 2018; Zhi et al., 2019), which was confirmed by the disordered relationship between matrix porosity and permeability (Fig. 2(a)). The distribution intervals of average matrix porosity of core samples with and without bedding-parallel fractures are shown in Fig. 2(b) and (c), respectively. The matrix porosity of core samples with bedding-parallel fractures was lower than that of samples without bedding-parallel fractures; most showed low matrix porosity (<6%), accounting for 46.8% of the total number of core samples with bedding-parallel fractures. This indicates that bedding-parallel fractures easily occurred in low matrix porosity rocks and suggests that the reservoir interval density of bedding-parallel fractures of low matrix porosity reservoirs is usually higher than that of reservoirs with high matrix porosity (Fig. 11). The average porosities of dolomite, dolomitic siltstone, and muddy siltstone reservoirs in the upper sweet spot of the Lucaogou Formation were 4.8%, 8.6%, and 11.6%, respectively. A distribution interval of reservoir interval density of bedding-parallel fractures can be seen in Fig. 12. The reservoir interval density of bedding-parallel fractures of dolomite reservoirs was the highest, followed by that of dolomitic siltstone and muddy siltstone reservoirs. Moreover, despite having similarly low porosities (6.5%, as marked by a green circle), the permeability of core samples with bedding-parallel fractures was significantly higher than that of rocks without bedding-parallel fractures (Fig. 2(a)). Bedding-parallel fractures appeared to be more developed in low matrix porosity reservoirs, which is consistent with the relationship between the reservoir interval density of bedding-parallel fractures and weighted matrix porosity of reservoir intervals (Fig. 12). In addition, the existence of bedding-parallel fractures increased the permeability by 1–2 orders of magnitude (Fig. 2(d) and (e)) in the absence of a monotonic correlation with the degree to which bedding-parallel fractures develop. Thus, the relationship between the degree to which bedding-parallel fractures develop (i.e., reservoir interval density of bedding-parallel fractures) and reservoir permeability was irregular (Fig. 17) and did not display an overall monotonic form. In conclusion, a higher correlation between the reservoir interval density of bedding-parallel fractures and matrix porosity suggests that the development of bedding-parallel fractures in fine-grained sedimentary rocks depends more on matrix porosity than on permeability. In terms of the mechanical process underlying bedding-parallel fracture formation, in case the mineral composition of fine-grained sedimentary rocks varies slightly, rocks with higher matrix porosity tend to exhibit lower brittleness characteristics (Baud et al., 2014; Heidari et al., 2014; Li et al., 2018). This is because the presence of pores weakens the overall mechanical structure of the tight fine-grained sedimentary rocks. Under the conditions of compression caused by tectonic stress, the pores tend to bear a portion of the stress, thereby reducing the internal stress and decreasing the overall strength of the rock (Shang et al., 2015; Askaripour et al., 2022). This makes the rock more susceptible to deformation rather than fracturing. In other words, a low matrix porosity favors the development of bedding-parallel fractures in fine-grained sedimentary rocks. Subsequently, these bedding-parallel fractures tend to increase the effective porosity of the reservoir to some extent.

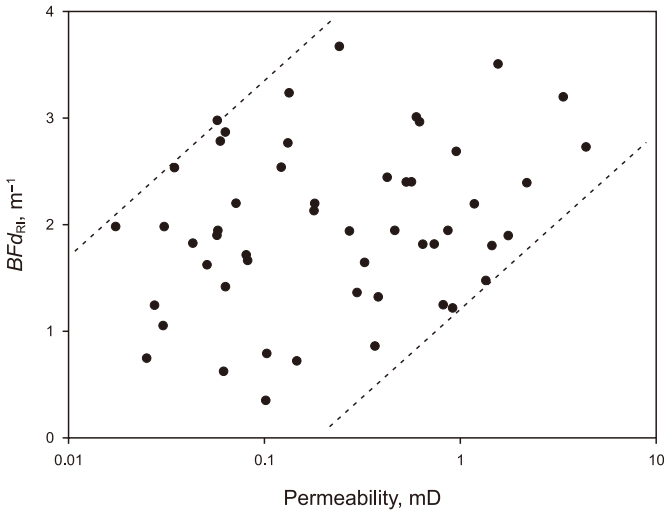

Fig. 17. Cross plots showing poor correlation between permeability and reservoir interval density of bedding-parallel fractures (BFd_{RI}) from the upper sweet spot interval of the Lucaogou Formation, Jimusar Sag.

The petroleum-bearing capacity in fine-grained sedimentary reservoirs was closely related to bedding-parallel fracture development (Jiang et al., 2013; Zhang et al., 2017; Lu et al., 2021; Pang et al., 2022; Du et al., 2023a), but it varied among bedding-parallel fractures. Under identical reservoir conditions (e.g., in-situ stress, temperature), variations in the oil-bearing capacities of bedding-parallel fractures were predominantly promoted by the formation and occurrence of bedding-parallel fractures and spatial coupling with source rocks (Xiang et al., 2013; Wang et al., 2020; Lu et al., 2021; Zeng et al., 2021). Most unfilled bedding-parallel fractures inside or near source-rocks were usually characterized by improved oil-bearing capacities. Oil-saturated, oil-immersed, and oil-potted core samples with high oil contents occurred frequently in the study area, while permeated crude oil and emissive natural gas were clearly observed along the bedding-parallel fractures (Fig. 18). In fine-grained sedimentary rock formations (e.g., shale), highly developed bedding-parallel fractures indicate high petroleum-bearing capacities and high contents of stored hydrocarbons.

5.3. Applicability of the proposed method for predicting the development of bedding-parallel fractures

Equations (1)–(6) present the mathematical calculation model of the parameters used for predicting the development of bedding-parallel fractures, while Fig. 4 shows the detailed process of implementation of the method. To highlight the applicability of the proposed method, the prediction of bedding-parallel fracture development was carried out in the upper sweet spot in the Lucaogou Formation; the results are shown in Fig. 12. For verifying the accuracy of the prediction method, the results of the reservoir interval density of bedding-parallel fractures were compared with the logging interpretation results from 22 reservoir intervals that were not included in the prediction model. The specific results are displayed in Table 1. The statistical results showed that the method for predicting the development of bedding-parallel fractures was well fitted for the Lucaogou Formation. Compared with the that in matched sweet spot density of bedding-parallel fractures based on interpretation results of FMI images, the average relative error of the prediction results was 8%. This acceptable value of error reveals that the method can be applied during the oil and gas exploration stages. Further analysis showed that the proposed method generally provided good results in predicting the development of bedding-parallel fractures (Table 1), but larger errors were observed mainly for the sweet spot comprising thinner reservoir intervals (<1.5 m). Hence, the accuracy of the proposed method was

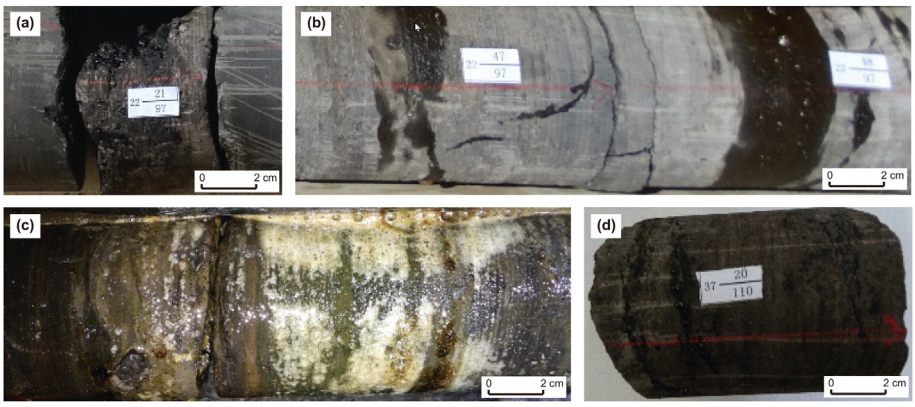

Fig. 18. Core photos in the J10025 well showing the seeping oil and gas along bedding-parallel fractures of the Lucaogou Formation. **(a)** 3615.5 m; **(b)** 3621.5 m; **(c)** 3718.9 m; **(d)** 3747.1 m.

Table 1
Error analysis of predicted sweet spot density of bedding-parallel fractures in the upper sweet spot of the Lucaogou Formation based on proposed methods.

No.	Well	Middle depth, m	$MBFd_s$, m^{-1}	$PBFd_s$, m^{-1}	Error r_1, m^{-1}	Error r_2, %
1	J38	2766.18	3.32	2.96	−0.36	11
2	J303	2398.45	3.14	3.26	0.12	4
3	J172	2830.81	2.98	3.18	0.20	7
4	J29	2312.37	2.96	3.02	0.06	2
5	J34	3553.33	2.64	2.33	−0.31	12
6	J174	3128.68	3.50	3.42	−0.08	2
7	J28	3149.38	0.98	1.12	0.14	15
8	J302	2783.89	2.06	1.89	−0.17	8
9	J36	4081.67	2.23	2.44	0.21	9
10	J27	2217.68	2.24	2.35	0.11	5
11	J30	3943.00	2.16	2.25	0.09	4
12	J25	3385.67	1.98	2.11	0.13	7
13	J41	3815.08	1.99	1.79	−0.20	10
14	J301	2717.19	1.96	2.13	0.17	8
15	J10060	4074.77	1.82	1.24	−0.58	32
16	J10038	3604.19	1.81	1.84	0.03	1
17	J10004	2571.48	1.73	1.98	0.25	14
18	J37	2796.14	1.64	1.70	0.06	4
19	J42	3267.78	1.30	1.18	−0.12	9
20	J10051	3711.15	1.76	1.88	0.12	7
21	J10035	3394.75	2.29	2.08	−0.21	9
22	J10016	3294.23	2.29	2.39	0.10	4
Average						8

Note: $MBFd_s$ is the matched sweet spot density of bedding-parallel fractures. $PBFd_s$ is the predicted sweet spot density of bedding-parallel fractures. The formula used for the

considerably affected by the matrix porosity and thickness of the reservoir interval. We suggest that, overall, the proposed method for predicting the development of bedding-parallel fractures based on matrix porosity (i.e., multi-scale matching and stepwise progressing methods) is practical and reliable.

Despite the applicability and reliability of proposed method in predicting the development of bedding-parallel fractures, its application has some limitations. The availability of core samples, the micro-resistivity scanning images and the quality of seismic data volume are the main limitations and sources of errors with proposed methodology in practice. Due to the complex and heterogeneous lithology of fine-grained sedimentary rocks, it can introduce errors in porosity evaluation and reservoir thickness interpretation results. We did not measure mineral composition by Litho Scanner Logging instrument, and herein, we mainly use conventional logging data to identify complex lithology. To reduce errors as much as possible, it would be worthwhile to upgrade the proposed mathematical model by building finer models for different lithology types and mechanical stratigraphy thickness in the future. The addition and combination resistivity, natural gamma, and mineral composition logs can consider the variation in lithology, mechanical property and offer more conclusive results.

5.4. Comparison of the methods for predicting the development of bedding-parallel fractures

The prediction of development of bedding-parallel fractures in fine-grained sedimentary reservoirs has attracted considerable attention in recent years, with various indirect methods being proposed (Bhattacharya et al., 2018; Basa et al., 2019; Lu et al., 2021; Dong et al., 2022; Lai et al., 2022). Compared with previous logging evaluation and seismic inversion methods, the method proposed in this study is a major step forward in the prediction of the development of bedding-parallel fractures. First, the logging evaluation methods (mainly including conventional logging and FMI) tend to focus on bedding-parallel fracture development near the borehole using the fracture number, line density, aperture and porosity but rarely consider interwell variations (Rajabi et al., 2010; Aghli et al.,

2016; Moreau and Joubert, 2016; Lai et al., 2022). As they are determined by comparing the accuracy of commonly used quantitative parameters for characterizing fractures, the fracture numbers interpreted by experts are more reliable than the computed fracture line density, aperture, and porosity based on FMI images or conventional logging. Presently, fracture number is mainly determined using the manually picked FMI images; intelligent auto-interpretation still remains a challenge. Second, the availability of 3D seismic data has revolutionized the study of faults and fractures and resulted in quantum advances in the understanding of the spatial and temporal distribution of such fractures. In particular, faults and fractures can be imaged with remarkable clarity with resolution down to ~m scale in some stances (Bahorich and Farmer, 1995; Crampin, 2003; Qi et al., 2017; Yuan et al., 2019; Dong et al., 2022; Bao et al., 2023). Plan view images of seismic attributes and seismic inversion substantially contribute to the spatial prediction of bedding-parallel fractures. Complementary cross-section images provide insights into temporal relationships as well as geological fault architecture. However, it is difficult to establish a statistical relationship between the commonly used seismic attribute parameters, such as curvature, anisotropic azimuthal, and coherence, and the absolute fracture number, owing to which the qualitative identification of macroscopic fracture development zones is based on relative values from seismic events. Accordingly, obtaining absolute developing degrees of bedding-parallel fractures with seismic methods is challenging (Abuamarah et al., 2019; Xu et al., 2020; Wei et al., 2021). Unlike the above-mentioned two common methods, the proposed method of multi-scale matching and stepwise progression combines the advantages of both the elements. This study improves our understanding of the development of bedding-parallel fractures and is expected to improve the reliability of the methods to predict the development of bedding-parallel fractures to a certain extent.

As a parameter applicable in both logging evaluation and seismic prediction, the reservoir interval density of bedding-parallel fractures is key for the spatial prediction of bedding-parallel fractures. A new approach to quantitatively describe the degree to which bedding-parallel fractures develop was revealed by improving the relationship between the reservoir interval density of bedding-parallel fractures and matrix porosity (Fig. 12). All intrinsic factors affecting bedding-parallel fracture development are related to lithological properties, such as brittle mineral contents, mechanical properties, and TOC contents (Zhang et al., 2018; Zeng et al., 2022). However, lithology is a descriptive variable in geology and is difficult to quantitatively apply in mathematical models (Donselaar and Schmidt, 2005; Corina and Hovda, 2018; Pang et al., 2022). Porosity seems to be the comprehensive response of these intrinsic factors affecting bedding-parallel fracture development, exhibiting the outstanding advantages of having abundant acquisition methods (e.g., calculation from logging curves, seismic attributes, seismic inversion) and reliable confidence (Lai et al., 2017; Wu et al., 2017; Yawar and Schieber, 2017; Dong et al., 2022). Equations (1)–(6) revealed that the accuracy of the proposed method was considerably affected by the matrix porosity and thickness of the reservoir interval. The proposed method generally provided good results in predicting the development of bedding-parallel fractures (Table 1), but the data with the largest error in the prediction results mainly came from the sweet spot comprising thinner reservoir intervals. Hence, it would be worthwhile to upgrade the proposed mathematical model by building finer models for different lithology types and mechanical stratigraphy thickness in the future.

5.5. Implications for the exploration of oil and gas in fine-grained sedimentary rocks

Bedding-parallel fractures are effective reservoir spaces and seepage paths for oil and gas, controlling their movement and accumulation as well as the productivity of individual wells (Loucks et al., 2009; McGinnis et al., 2017; Basa et al., 2019; Momeni et al., 2019; Liang et al., 2021; Lu et al., 2021; Zeng et al., 2024). Oil and gas seepage along bedding-parallel fractures on core samples revealed the effectiveness of the bedding-parallel fractures (Fig. 18); by observing the cores, it is easy to estimate the petroleum-bearing capacity of individual bedding-parallel fractures. Furthermore, we found that the better the oil-bearing capacity of a bedding-parallel fracture in fine-grained sedimentary rocks, the better is the quality of the surrounding reservoir. However, when the number of core samples available is limited, investigating all reservoir intervals is challenging. Fortunately, those reservoirs with higher reservoir interval density of bedding-parallel fractures generally present a high oil-bearing capacity in the study area (Figs. 11 and 14) and have a large production capacity. Therefore, we consider that the reservoir interval density of bedding-parallel fractures is an ideal indirect indicator of the quality of fine-grained sedimentary reservoirs and represents a crucial parameter in oil and gas exploration.

To further clarify the relationship between the reservoir interval density of bedding-parallel fractures and reservoir productivity, logging interpretation reservoir types were employed. Reservoir quality was categorized according to oil saturation and ranked as follows: Class I > Class II > Class III > Class IV. These reservoir types were counted based on the results of the evaluation and prediction of the reservoir interval density of bedding-parallel fractures in the Lucaogou Formation. Based on the data from 69 reservoirs from 27 wells, the relationships between reservoir interval density of

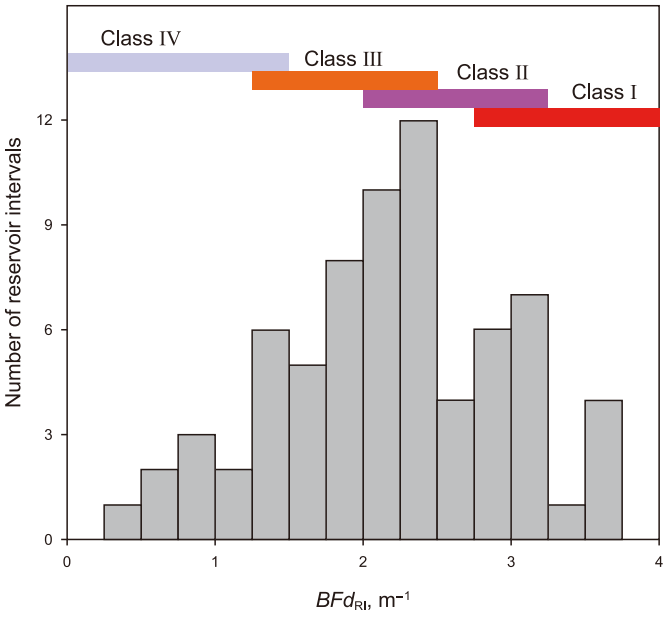

Fig. 19. The distribution histogram of the reservoir interval density of bedding-parallel fractures (BFd_{RI}) illustrates the influence of bedding-parallel fracture development on oil-bearing properties; as the reservoir interval density of bedding-parallel fractures increases, the oil-bearing capacity increases. Oil layer ranked as Class I > Class II > Class III > Class IV.

bedding-parallel fractures and reservoir types are presented in Fig. 19. A high correspondence was observed between the two, as the reservoir rank increased with an increase in the reservoir interval density of bedding-parallel fractures. These results indicate that the reservoir interval density of bedding-parallel fractures is an effective indicator of the production capacity of fine-grained sedimentary rocks in the Lucaogou Formation in Jimusar Sag.

6. Conclusions

Bedding-parallel fractures have extensively developed in the fine-grained sedimentary reservoirs in the Lucaogou Formation. They tend to occur in preexisting weaker bedding planes and interfaces between lithologies. Unfilled bedding-parallel fractures inside or near source-rocks are usually characterized by better oil-bearing capacity, and they are identified on FMI images by regularly continuous sinusoidal black or nearly black curves. The degree of the development of bedding-parallel fractures is positively related to the brittle mineral and total organic carbon contents and negatively related to single reservoir interval thickness. Furthermore, the occurrence of faults also plays a promoting role to a certain extent.

Reservoir interval density of bedding-parallel fractures and matched reservoir interval density of bedding-parallel fractures from conventional logging datasets and FMI images were employed to quantitatively characterize the degree to which bedding-parallel fractures and heterogeneity develop in fine-grained sedimentary rocks. The matched sweet spot density of bedding-parallel fractures was combined to establish a novel approach for predicting the degree of development and the planar distribution of bedding-parallel fractures based on 3D seismic data. This paper outlines an effective and practical approach to predict the degree to which bedding-parallel fractures develop as well as their spatial distribution. A univariate model employing matrix porosity was established to determine the reservoir interval density of bedding-parallel fractures. The vertical evaluation of the development of bedding-parallel fractures in individual wells was achieved by interpreting the quantitative parameters of bedding-parallel fractures in fine-grained sedimentary rocks. Subsequently, their planar distribution was predicted using multi-scale matching and step-by-step progressive methods. The proposed methods were applied to the Permian Lucaogou Formation, and produced favorable results, with a stronger adaptability than that of previously proposed methods, underscoring their wide application. Furthermore, the proposed parameters enhance the quantitative contrasting capability of bedding-parallel fractures as well as upgrade their multi-scale quantification characterization, making them indicative for the fine prediction of reservoirs in fine-grained sedimentary rocks.

Conflicts of interest

All authors have approved the submission of this manuscript. The results have not been previously published and are not being considered for publication in another journal simultaneously. We also confirm that there is no interest of conflict needed to be claimed, and all the funding sources have been mentioned in the manuscript.

CRediT authorship contribution statement

Zhao-Hui Zhang: Writing – review & editing, Funding acquisition, Formal analysis, Conceptualization. **Teng Zhang:** Writing – original draft, Software, Resources, Conceptualization. **Hua-Qing Liu:** Supervision, Project administration, Funding acquisition. **Xiang-Bo Li:** Writing – review & editing, Project administration, Methodology. **Duo-Nian Xu:** Visualization, Funding acquisition, Conceptualization.

Acknowledgements

We would like to thank the editors and anonymous reviewers; their informative and constructive comments and suggestions improved the study. Samples were provided by Xinjiang Oilfiled Company of Petrochina, and Zhundong Petroleum Technology Co., Ltd. We thank them for their help with this study and for their agreement to publication of the results. This work was financially supported by the National Natural Science Foundation of China (No. 41872116), National Science and Technology Major Project (No. 2017ZX05001-003), Initial Scientific Research Foundation of Xinjiang University for Doctor (No. 620321016), and Research Foundation of Tianchi Outstanding Doctor (No. 51052300560).

References

Abuamarah, B.A., Nabawy, B.S., Shehata, A.M., et al., 2019. Integrated geological and petrophysical characterization of Oligocene deep marine unconventional poor to tight sandstone gas reservoir. Mar. Petrol. Geol. 109, 868–885. https://doi.org/10.1016/j.marpetgeo.2019.06.037.

Aghli, G., Soleimani, B., Moussavi-Harami, R., Mohammadian, R., 2016. Fractured zones detection using conventional petrophysical logs by differentiation method and its correlation with image logs. J. Petrol. Sci. Eng. 142, 152–162. https://doi.org/10.1016/j.petrol.2016.02.002.

Altawati, F., Emadi, H., Pathak, S., 2021. Improving oil recovery of Eagle Ford shale samples using cryogenic and cyclic gas injection methods-an experimental study. Fuel 302, 121170. https://doi.org/10.1016/j.fuel.2021.121170.

Aplin, A.C., Macquaker, J.H., 2011. Mudstone diversity: origin and implications for source, seal, and reservoir properties in petroleum systems. AAPG Bull. 95 (12), 2031–2059. https://doi.org/10.1306/03281110162.

Askaripour, M., Saeidi, A., Mercier-Langevin, P., Rouleau, A., 2022. A Review of relationship between texture characteristic and mechanical properties of rock. Geotechnics 2, 262–296. https://doi.org/10.3390/geotechnics2010012.

Bahorich, M., Farmer, S., 1995. 3-D seismic discontinuity for faults and stratigraphic features; the coherence cube. Lead. Edge. 14 (10), 1053–1058. https://doi.org/10.1190/1.1437077.

Bao, M.Y., Dong, S.Q., Zeng, L.B., He, J., Sun, F.T., Han, G.S., 2023. Artificial intelligence prediction method for tight carbonate reservoir fracture distribution based on seismic attributes. Earth Sci. 48 (7), 2462–2474. https://doi.org/10.3799/dqkx.2022.290 (in Chinese).

Basa, A., Ahmed, F., Bhattacharyya, K., Roy, A., 2019. Evolution and characterization of fracture patterns: insights from multi-scale analysis of the Buxa dolomite in the Siang Valley, Arunachal Lesser Himalayan fold-thrust belt. J. Struct. Geol. 123, 54–66. https://doi.org/10.1016/j.jsg.2019.03.004.

Baud, P., Wong, T.F., Zhu, W., 2014. Effects of porosity and crack density on the compressive strength of rocks. Int. J. Rock Mech. Min. Sci. 67, 202–211. https://doi.org/10.1016/j.ijrmms.2013.08.031.

Bergbauer, S., Pollard, D.D., 2004. A new conceptual foldfracture model including prefolding joints, based on the Emigrant Gap anticline, Wyoming. AAPG Bull. 116 (3), 294–307. https://doi.org/10.1130/B25225.1.

Bhattacharya, S., Mishra, S., 2018. Applications of machine learning for facies and fracture prediction using bayesian network theory and random forest: case studies from the appalachian basin, USA. J. Petrol. Sci. Eng. 170, 1005–1017. https://doi.org/10.1016/j.petrol.2018.06.075.

Cao, Z., Liu, G.D., Kong, Y.H., Wang, C.Y., Niu, Z.C., Zhang, J.Y., Geng, C.B., Shan, X., Wei, Z.P., 2016. Lacustrine tight oil accumulation characteristics: permian Lucaogou Formation in jimusaer sag, Junggar Basin. Int. J. Coal Geol. 135, 37–51. https://doi.org/10.1016/j.coal.2015.11.004.

Chen, L.C., Tan, J.Q., Cui, H.S., Ma, X., Song, X.Q., Yuan, Q., Liu, J., 2023. Hydrocarbon generation mechanism of lamalginite- and telalginite-dominated source rocks in a saline lake basin: a case study of the Permian Lucaogou formation in the Jimusaer Sag, Junggar Basin. Energy Geoscience 4, 100191. https://doi.org/10.1016/j.engeos.2023.100191.

Chen, Z.H., Cao, Y.C., Wang, X.L., Qiu, L.W., Tang, Y., Yuan, G.H., 2016. Oil origin and accumulation in the Paleozoic Chepaizie-Xinguang field, Junggar basin, China. J. Asian Earth Sci. 115, 1–15. https://doi.org/10.1016/j.jseaes.2015.09.019.

Cobbold, P.R., Zanella, A., Rodrigues, N., Løseth, H., 2013. Bedding-parallel fibrous veins (beef and cone-in-cone): worldwide occurrence and possible significance in terms of fluid overpressure, hydrocarbon generation and mineralization. Mar. Petrol. Geol. 43, 1–20. https://doi.org/10.1016/j.marpetgeo.2013.01.010, 2013.

Corina, A.N., Hovda, S., 2018. Automatic lithology prediction from well logging using kernel density estimation. J. Petrol. Sci. Eng. 170, 664–674. https://doi.org/10.1016/j.petrol.2018.06.012.

Crampin, S., 2003. The new geophysics: shear-wave splitting provides a window into the crack-critical rock mass. Lead. Edge 22, 536–549. https://doi.org/10.1190/1.1587673.

Du, X.Y., Jin, Z.J., Zeng, L.B., Liu, G.P., He, W.J., Ostadhassan, M., Liang, X.P., Yang, S., Lu, G.Q., 2023a. Characteristics and controlling factors of natural fractures in deep lacustrine shale oil reservoirs of the Permian Fengcheng Formation in the Mahu Sag, Junggar Basin, China. J. Struct. Geol. 175, 104923. https://doi.org/10.1016/j.jsg.2023.104923.

Du, X.Y., Jin, Z.J., Zeng, L.B., Liu, G.P., He, W.J., Ostadhassan, M., Song, Y., Liang, X.P., Yang, S., Lu, G.Q., 2023b. Formation of natural fractures and their impact on shale oil accumulation in the Mahu Sag, Junggar Basin, NW China. Int. J. Coal Geol. 279, 104385. https://doi.org/10.1016/j.coal.2023.104385.

Dong, S.Q., Zeng, L.B., Du, X.Y., Bao, M.Y., Lyu, W.Y., Ji, C.Q., Hao, J.R., 2022. An intelligent prediction method of fractures in tight carbonate reservoirs. Petrol. Explor. Dev. 49 (4), 1–11. https://doi.org/10.1016/S1876-3804(23)60355-6.

Donselaar, M.E., Schmidt, J.M., 2005. Integration of outcrop and borehole image logs for high-resolution facies interpretation: example from a fluvial fan in the Ebro Basin, Spain. Sedimentology 52, 1021–1042. https://doi.org/10.1111/j.1365-3091.2005.00737.x.

Espejel, R.L., Alves, T.M., Blenkinsop, T.G., 2020. Multi-scale fracture network characterisation on carbonate platforms. J. Struct. Geol. 140, 104160. https://doi.org/10.1016/j.jsg.2020.104160.

Ezati, M., Olfati, H., Khadem, M., Yazdanipour, M.R., Mohammad, A., 2019. Petrophysical evaluation of a severely heterogeneous carbonate reservoir; Electrical image logs usage in porosity estimation. Open J. Geol. 9, 193–200. https://doi.org/10.4236/ojg.2019.93013.

Feng, D., Chen, D.F., 2015. Authigenic carbonates from an active cold seep of the northern South China Sea: new insights into fluid sources and past seepage activity. Deep Sea Res. Part II Top. Stud. Oceanogr. 122, 74–83. https://doi.org/10.1016/j.dsr2.2015.02.003.

Folkestad, A., Veselovsky, Z., Roberts, P., 2012. Utilising borehole image logs to interpret delta to estuarine system: a case study of the subsurface Lower Jurassic Cook Formation in the Norwegian northern North Sea. Mar. Petrol. Geol. 29 (1), 255–275. https://doi.org/10.1016/j.marpetgeo.2011.07.008.

Gale, J.F.W., Laubach, S.E., Olson, J.E., Eichhubl, P., Fall, A., 2014. Natural fractures in shale: a review and new observations. AAPG Bull. 98 (11), 2165–2216. https://doi.org/10.1306/08121413151.

Gao, H., Li, H.A., 2016. Pore structure characterization, permeability evaluation and enhanced gas recovery techniques of tight gas sandstones. J. Nat. Gas Sci. Eng. 28, 536–547. https://doi.org/10.1016/j.jngse.2015.12.018.

Gasparrini, M., Lacombe, O., Rohais, S., Belkacemi, M., Euzen, T., 2021. Natural mineralized fractures from the Montney-Doig unconventional reservoirs (Western Canada Sedimentary Basin): timing and controlling factors. Mar. Petrol. Geol. 124, 104826. https://doi.org/10.1016/j.marpetgeo.2020.104826.

Ghadeer, S.G., Macquaker, J.H., 2011. Sediment transport processes in an ancient muddominated succession: a comparison of processes operating in marine offshore settings and anoxic basinal environments. J. Geol. Soc. 168 (5), 1121–1132. https://doi.org/10.1144/0016-76492010-016.

Gou, Q.Y., Xu, S., Hao, F., Yang, F., Zhang, B.Q., Shu, Z.G., Zhang, A.H., Wang, Y.X., Lu, Y.B., Cheng, X., Qing, J.W., Gao, M.T., 2019. Full-scale pores and micro-fractures characterization using FE-SEM, gas adsorption, nano-CT and micro-CT: a case study of the Silurian Longmaxi Formation shale in the Fuling area, Sichuan Basin, China. Fuel 253, 167–179. https://doi.org/10.1016/j.fuel.2019.04.116.

Gu, Y., Ding, W.L., Tian, Q.N., Xu, S., Zhang, W., Zhang, B.R., Jiao, B.C., 2020. Developmental characteristics and dominant factors of natural fractures in lower Silurian marine organic-rich shale reservoirs: a case study of the Longmaxi formation in the Fenggang block, southern China. J. Petrol. Sci. Eng. 192, 107277. https://doi.org/10.1016/j.petrol.2020.107277.

Heidari, M., Khanlari, G.R., Torabi-Kaveh, M., Kargarian, S., Saneie, S., 2014. Effect of porosity on rock brittleness. Rock Mech. Rock Eng. 47, 785–790. https://doi.org/10.1007/s00603-013-0400-0.

Heng, S., Li, X.Z., Liu, X., Chen, Y., 2020. Experimental study on the mechanical properties of bedding planes in shale. J. Nat. Gas Sci. Eng. 76, 103161. https://doi.org/10.1016/j.jngse.2020.103161.

Hooker, J.N., Abu-Mahfouza, I.S., Meng, Q., Cartwright, J., 2019. Fractures in mudrocks: advances in constraining timing and understanding. J. Struct. Geol. 125, 166–173. https://doi.org/10.1016/j.jsg.2018.04.020.

Huang, J.X., Peng, S.M., Wang, X.J., Xiao, K., 2006. Applications of imaging logging data in the research of fracture and ground stress. Acta Pet. Sin. 27 (6), 65–69. https://doi.org/10.1016/S1872-2040(06)60004-2 (in Chinese).

Jiang, Z.X., Liang, C., Wu, J., Zhang, J.G., Zhang, W.Z., Wang, Y.S., Liu, H.M., Xiang, C., 2013. Several issues in sedimentological studies on hydrocarbon-bearing fine-grained sedimentary rocks. Acta Pet. Sin. 34 (6), 1031–1039. https://doi.org/10.1016/S1876-3804(18)30064-8 (in Chinese).

Ju, W., You, Y., Feng, S.B., Xu, H.R., Zhang, X.L., Wang, S.Y., 2020. Characteristics and genesis of bedding-parallel fractures in tight sandstone reservoirs of Chang 7 oil layer, Ordos Basin. Oil Gas Geol. 41 (3), 596–605. https://doi.org/10.11743/ogg20200315 (in Chinese).

Keeton, G., Pranter, M., Cole, R.D., 2015. Stratigraphic architecture of fluvial deposits from borehole images, spectral-gamma-ray response, and outcrop analogs, Piceance Basin, Colorado. AAPG Bull. 99 (10), 1929. https://doi.org/10.1306/05071514025.

Krumbein, W.C., 1947. Shales and their environmental significance. J. Sediment. Res. 17 (3), 10. https://doi.org/10.1306/D42692BF-2B26-11D7-8648000102C1865D.

Kuang, L.C., Tang, Y., Lei, D.W., Ouyang, M., Hou, L.H., Liu, D.G., 2012. Formation conditions and exploration potential of tight oil in the Permian saline lacustrine dolomitic rock, Junggar Basin, NW China. Petrol. Explor. Dev. 39 (6), 657–667. https://doi.org/10.1016/S1876-3804(12)60095-0.

Kuang, L.C., Wang, X.T., Guo, X.G., Chang, Q.S., Jia, X.Y., 2019. Geological characteristics and exploration practice of tight oil of Lucaogou Formation in Jimusar Sag. Xinjing Pet. Geol. 36 (6), 629–634. https://doi.org/10.7657/XJPG20150601 (in Chinese).

Lacombe, O., Bellahsen, N., Mouthereau, F., 2011. Fracture patterns in the Zagros Simply Folded Belt (Fars, Iran): constraints on early collisional tectonic history and role of basement faults. Geol. Mag. 148 (5–6), 940–960. https://doi.org/10.1017/S001675681100029X.

Lai, J., Liu, B.C., Li, H.B., Pang, X.J., Liu, S.C., Mao, M., 2022. Bedding parallel fractures in fine-grained sedimentary rocks: recognition, formation mechanisms, and prediction using well log. Petrol. Sci. 19, 554–569. https://doi.org/10.1016/j.petsci.2021.10.017.

Lai, J., Wang, G.W., Fan, Z.Y., Wang, Z.Y., Chen, J., Zhou, Z.L., Wang, S.W., Xiao, C.W., 2017. Fracture detection in oil-based drilling mud using a combination of borehole image and sonic logs. Mar. Petrol. Geol. 84, 195–214. https://doi.org/10.1016/j.marpetgeo.2017.03.035.

Lai, J., Wang, G.W., Sun, S.M., Jiang, C., Zhou, L., Zheng, X.H., Wu, Q.K., Han, C., 2015. Research advances in logging recognition and evaluation method of fractures in tight sandstone reservoirs. Prog. Geophys. 30 (4), 1712–1724. https://doi.org/10.6038/pg20150426 (in Chinese).

Li, H.M., Li, H.G., Wang, K.L., Liu, C., 2018. Effect of rock composition microstructure and pore characteristics on its rock mechanics properties. Int. J. Min. Sci. Technol. 28 (2), 303–308. https://doi.org/10.1016/j.ijmst.2017.12.008.

Li, L.H., Huang, B.X., Li, Y.Y., Shao, P., Gao, X.B., Hu, R.L., Li, X., 2018. Multi-scale modeling of shale laminaes and fracture networks in the Yanchang formation, southern Ordos basin, China. Eng. Geol. 243, 231–240. https://doi.org/10.1016/j.enggeo.2018.07.010.

Li, Z.X., Liu, Y.Q., Jiao, X., Zhou, D.W., Yang, Y.Y., You, J.Y., 2019. Progress and present research on volcanic-hydrothermal related fine-grained sedimentary rocks. J. Palaeogeogr. 21 (5), 727–742. https://doi.org/10.7605/gdlxb.2019.05.049.

Liang, M.L., Wang, Z.X., Zhang, Y., Greenwell, C.H., Li, H.J., Yu, Y.X., Liu, S.X., 2021. Experimental investigation on gas permeability in bedding shale with brittle and semi-brittle deformations under triaxial compression. J. Petrol. Sci. Eng. 196, 108049. https://doi.org/10.1016/j.petrol.2020.108049.

Lin, M.R., Xi, K.L., Cao, Y.C., Liu, Q.Y., Zhang, Z.H., Li, K., 2021. Petrographic features and diagenetic alteration in the shale strata of the permian Lucaogou Formation, jimusar sag, Junggar Basin. J. Petrol. Sci. Eng. 203, 108684. https://doi.org/10.1016/j.petrol.2021.108684.

Liu, B., Bechtel, A., Sachsenhofer, R.F., Gross, D., Gratzer, R., Chen, X., 2017. Depositional environment of oil shale within the second member of permian Lucaogou Formation in the santanghu basin, NW China. Int. J. Coal Geol. 175, 10–25. https://doi.org/10.1016/j.coal.2017.03.011.

Liu, B., Sun, J.H., Zhang, Y.Q., He, J.L., Fu, X.F., Yang, L., Xing, J.L., Zhao, X.Q., 2021. Reservoir space and enrichment model of shale oil in the first member of Cretaceous Qingshankou Formation in the Changling Sag, southern Songliao Basin, NE China. Petrol. Explor. Dev. 48 (3), 608–624. https://doi.org/10.1016/S1876-3804(21)60049-6.

Liu, B., Wang, H.L., Fu, X.F., Bai, Y.F., Bai, L.H., Jia, M.C., He, B., 2019. Lithofacies and depositional setting of a highly prospective lacustrine shale oil succession from the Upper Cretaceous Qingshankou Formation in the Gulong Sag, northern Songliao Basin, NE China. AAPG (Am. Assoc. Pet. Geol.) Bull. 103 (2), 405–432. https://doi.org/10.1306/08031817416.

Liu, G.P., Lin, Z.J., Zeng, L.B., Huang, L.L., Ostadhassan, M., Du, X.Y., Lu, G.Q., Zhang, Y.Z., 2023. Natural fractures in deep continental shale oil reservoirs: a case study from the Permian Lucaogou formation in the Eastern Junggar Basin, Northwest China. J. Struct. Geol. 174, 104913. https://doi.org/10.1016/j.jsg.2023.104913.

Liu, H.P., Zhang, C.M., Zhang, L., Luo, Y., 2022. Bedding-parallel fractures in ultradeep tight sandstone reservoirs in jurassic and cretaceous of yongjin oil field, Junggar Basin, China. Front. Earth Sci. 16, 975–988. https://doi.org/10.1007/s11707-022-0999-9.

Liu, D.D., Zhang, C., Pan, Z.K., Huang, Z.X., Luo, Q., Song, Y., Jiang, Z.X., 2020. Natural fractures in carbonate-rich tight oil reservoirs from the Permian Lucaogou Formation, southern Junggar Basin, NW China: insights from fluid inclusion microthermometry and isotopic geochemistry. Mar. Petrol. Geol. 119, 104500. https://doi.org/10.1016/j.marpetgeo.2020.104500.

Loucks, R.G., Reed, R.M., Ruppel, S.C., Jarvie, D.M., 2009. Morphology, genesis, and distribution of nanometer-scale pores in siliceous mudstones of the Mississippian Barnett shale. J. Sediment. Res. 79, 848–861. https://doi.org/10.2110/jsr.2009.092.

Lu, G.Q., Zeng, L.B., Dong, S.Q., Huang, L.L., Liu, G.P., Ostadhassan, M., He, W.J., Du, X.Y., Bao, C.P., 2023. Lithology identification using graph neural network in continental shale oil reservoirs: a case study in Mahu Sag, Junggar Basin, Western China. Mar. Petrol. Geol. 150, 106168. https://doi.org/10.1016/j.marpetgeo.2023.106168.

Lu, J., Zhang, C., Zeng, J.H., Yuan, H.W., 2021. Research on the oil-bearing difference of bedding fractures: a case study of Lucaogou Formation in Jimusar Sag. Geofluids 5567491. https://doi.org/10.1155/2021/5567491.

Luo, Q., Wei, Y.H., Liu, D.D., Zhang, C., Zhu, D.Y., Zhang, Y.Z., Wang, J., 2017. Research significance, advances and trends on the role of bedding fracture in tight oil accumulation. Petrol. Geo. Exp. 39 (1), 1–7. https://doi.org/10.11781/sysydz201701001 (in Chinese).

Lyu, W.Y., Zeng, L.B., Zhang, B.J., Miao, F.B., Lyu, P., Dong, S.Q., 2017. Influence of natural fractures on gas accumulation in the Upper Triassic tight gas sandstones

in the northwestern Sichuan Basin. China. Mar. Petrol. Geol. 83, 60–72. https://doi.org/10.1016/j.marpetgeo.2017.03.004.
Ma, K., Hou, J.G., Liu, Y.M., Shi, Y.Q., Lin, Y., Chen, F.L., 2017. The sedimentary model of saline lacustrine mixed sedimentation in Permain Lucaogou Formation, Jimusar Sag. Acta Pet. Sin. 38 (6), 636–648. https://doi.org/10.7623/syxb201706003 (in Chinese).
Ma, Y., Pan, Z.J., Zhong, N.N., Connell, L.D., Down, D.I., Lin, W.L., Zhang, Y., 2016. Experimental study of anisotropic gas permeability and its relationship with fracture structure of Longmaxi Shales, Sichuan Basin, China. Fuel 180 (15), 106–115. https://doi.org/10.1016/j.fuel.2016.04.029.
McGinnis, R.N., Ferrill, D.A., Morris, A.P., Smart, K.J., Lehrmann, D., 2017. Mechanical stratigraphic controls on natural fracture spacing and penetration. J. Struct. Geol. 95, 160–170. https://doi.org/10.1016/j.jsg.2017.01.001.
Mohammed, I., Olayiwola, T.O., Alkathim, M., Awotunde, A.A., Alafnan, S.F., 2021. A review of pressure transient analysis in reservoirs with natural fractures, vugs and/or caves. Petrol. Sci. 18, 154–172. https://doi.org/10.1007/s12182-020-00505-2.
Momeni, A., Rostamia, S., Hashemi, Mosalman-Nejadc, H., Ahmadic, A., 2019. Fracture and fluid flow paths analysis of an offshore carbonate reservoir using oil-based mud images and petrophysical logs. Mar. Petrol. Geol. 109, 349–360. https://doi.org/10.1016/j.marpetgeo.2019.06.021.
Moreau, J., Joubert, J.B., 2016. Glacial sedimentology interpretation from borehole image log: example from the Late Ordovician deposits, Murzuq Basin (Libya). Interpretation 4 (2), B1–B16. https://doi.org/10.1190/int-2015-0161.1.
Nabawy, B.S., Elgendy, N.T.H., Gazia, M.T., 2020. Mineralogic and diagenetic controls on reservoir quality of paleozoic sandstones, gebel el-zeit, north eastern desert, Egypt. Nat. Resour. Res. 29 (2), 1215–1238. https://doi.org/10.1007/s11053-019-09487-4.
Nian, T., Wang, G.W., Cang, D., Tan, C.Q., Tan, Y.H., Zhang, F.S., 2022. The diagnostic criteria of borehole electrical imaging log for volcanic reservoir interpretation: an example from the Yingcheng Formation in the Xujiaweizi Depression, Songliao Basin, China. J. Petrol. Sci. Eng. 208, 109713. https://doi.org/10.1016/j.petrol.2021.109713.
Niu, D.M., Li, Y.L., Zhang, Y.F., Sun, P.C., Wu, H.G., Fu, H., Wang, Z.Q., 2022. Multi-scale classification and evaluation of shale reservoirs and 'sweet spot' prediction of the second and third members of the Qingshankou Formation in the Songliao Basin based on machine learning. J. Petrol. Sci. Eng. 216, 110678. https://doi.org/10.1016/j.petrol.2022.110678.
Niu, X.B., Feng, S.B., You, Y., Xin, H.G., Liang, X.W., Hao, B.Y., Dan, W.D., 2022. Analyzing major controlling factors of shale oil 'sweet spots' in the Chang-7 member of the Triassic Yanchang Formation, Ordos Basin. Unconvent. Resour. 2, 51–59. https://doi.org/10.1016/j.uncres.2022.07.001.
Pang, X.J., Wang, G.W., Kuang, L.C., Li, H.B., Zhao, Y.D., Li, D., Zhao, X., Wu, S.T., Feng, Z., Lai, J., 2022. Insights into the pore structure and oil mobility in fine-grained sedimentary rocks: the Lucaogou Formation in Jimusar Sag, Junggar Basin. China. Mar. Petrol. Geol. 137, 105492. https://doi.org/10.1016/j.marpetgeo.2021.105492.
Parnell, J., Carey, P.F., Monson, B., 1996. Fluid inclusion constraints on temperatures of petroleum migration from authigenic quartz in bitumen veins. Chem. Geol. 129 (3–4), 216–217. https://doi.org/10.1016/0009-2541(95)00141-7.
Poppelreiter, M., García-Carballido, C., Kraaijveld, M., 2010. Borehole image log technology: application across the exploration and production life cycle. In: Dipmeter and Borehole Image Log Technology, vol. 92. AAPG Memoir, pp. 1–13. https://doi.org/10.1306/13181274M923406.
Qi, J., Li, F.Y., Marfurt, k., 2017. Multiazimuth coherence. Geophysics 82 (6), O83–O89. https://doi.org/10.1190/geo2017-0196.1.
Qiu, Z., Shi, Z.S., Dong, D.Z., Lu, B., Zhang, C.C., Zhou, J., Wang, H.Y., Xiong, B., Pang, Z.L., Guo, H.K., 2016. Geological characteristics of source rock and reservoir of tight oil and its accumulation mechanism: a case study of Permian Lucaogou Formation in Jimusar sag, Junggar Basin. Petrol. Explor. Dev. 43 (6). https://doi.org/10.1016/S1876-3804(16)30118-5, 1034–1024.
Qu, H.Z., Zhang, F.X., Wang, Z.Y., Yang, X.T., Liu, H.T., Ba, D., Wang, X., 2016. Quantitative fracture evaluation method based on core-image logging: a case study of Cretaceous Bashijiqike Formation in ks2 well area, Kuqa depression, Tarim Basin, NW China. Petrol. Explor. Dev. 43 (3), 465–473. https://doi.org/10.1016/S1876-3804(16)30054-4.
Rajabi, M., Sherkati, S., Bohloli, B., Tingay, M., 2010. Subsurface fracture analysis and determination of in-situ stress direction using FMI logs: an example from the Santonian carbonates (Ilam Formation) in the Abadan Plain, Iran. Tectonophysics 492 (1–4), 192–200. https://doi.org/10.1016/j.tecto.2010.06.014.
Savin, C., Grasso, J.R., Bachelery, P., 2005. Seismic signature of a phreatic explosion: hydrofracturing damage at Karthala volcano, grande comore Island. Indian Ocean. Bull. Volcanol. 67, 717–731. https://doi.org/10.1007/s00445-005-0411-0.
Schulz, R., Buness, H., Gabriel, G., Pucher, R., Rolf, C., Wiederhold, H., Wonik, T., 2005. Detailed investigation of preserved maar structures by combined geophysical surveys. Bull. Volcanol. 68, 95–106. https://doi.org/10.1007/s00445-005-0424-8.
Serra, O., 1989. Formation Microscanner Image Interpretation. Schlumberger Educational Services, Houston Texas, p. 117.
Shang, J.L., Hu, J.H., Zhou, K.P., Luo, X.W., Aliyu, M.M., 2015. Porosity increment and strength degradation of low-porosity sedimentary rocks under different loading conditions. Int. J. Rock Mech. Min. Sci. 75, 216–233. https://doi.org/10.1016/j.ijrmms.2015.02.002.
Shang, X.F., Long, S.X., Duan, T.Z., 2021. Fracture system in shale gas reservoir: prospect of characterization and modeling techniques. J. Nat. Gas Geo. 6 (3), 157–172. https://doi.org/10.1016/j.jnggs.2021.06.001.
Shi, L., Wang, X.Z., Bojiang, F., Lv, L., Li, Y.T., Yang, S., 2018. Characteristics of sandy lamination and its hydrocarbon accumulation, yanchang formation, Ordos basin. Oil Gas Geol. 39 (3), 522–530. https://doi.org/10.11743/ogg20180309.
Shi, Z.S., Qiu, Z., 2021. Main bedding types of marine fine-grained sediments and their significance for oil and gas exploration and development. Acta Sedimentol. Sin. 39 (1), 181–196. https://doi.org/10.14027/j.issn.1000-0550.2020.097 in Chinese.
Su, A., Bons, P.D., Chen, H.H., Feng, Y.X., Zhao, J.X., Song, J.W., 2022. Age, material source, and formation mechanism of bedding-parallel calcite beef veins: case from the mature Eocene lacustrine shales in the Biyang Sag, Nanxiang Basin, China. GSA Bulletin 134 (7–8), 1811–1833. https://doi.org/10.1130/B35866.1.
Tadayoni, M., Khalilbeyg, M., Junin, R.B., 2020. A new approach to heterogeneity analysis in a highly complex carbonate reservoir by using borehole image and conventional log data. J. Pet. Explor. Prod. Technol. 10, 2613–2629. https://doi.org/10.1007/s13202-020-00930-4.
Tong, X.G., Zhang, G.Y., Wang, Z.M., Wen, Z.X., Tian, Z.J., Wang, H.J., Ma, Feng, Wu, Y.P., 2018. Distribution and potential of global oil and gas resources. Petrol. Explor. Dev. 45 (4), 779–789. https://doi.org/10.1016/S1876-3804(18)30081-8.
Wang, Q.T., Liu, W.H., Pei, L.X., Cai, Z.H., Luo, H.Y., Wang, X.F., Zhang, D.D., Liu, J.Z., 2021. Hydrocarbon generation from calcium stearate: insights from closed-system pyrolysis. Mar. Petrol. Geol. 126, 104923. https://doi.org/10.1016/j.marpetgeo.2021.104923.
Wang, Y.C., Cao, J., Tao, K.Y., Li, E.T., Ma, C., Shi, C.H., 2020. Reevaluating the source and accumulation of tight oil in the middle permian Lucaogou Formation of the Junggar Basin. China. Mar. Petrol. Geol. 117, 104384. https://doi.org/10.1016/j.marpetgeo.2020.104384.
Wei, Y.S., Wang, J.L., Yu, W., Qi, Y.D., Miao, J.J., Yuan, H., Liu, C.X., 2021. A smart productivity evaluation method for shale gas wells based on 3D fractal fracture network model. Petrol. Explor. Dev. 48 (4), 787–796. https://doi.org/10.1016/S1876-3804(21)60076-9.
Wilson, M.E.J., Lewis, D., Yogi, O., Holland, D., Hombo, L., Goldberg, A., 2013. Development of a Papua New Guinean onshore carbonate reservoir: a comparative borehole image (FMI) and petrographic evaluation. Mar. Petrol. Geol. 44, 164–195. https://doi.org/10.1016/j.marpetgeo.2013.02.018.
Wu, J., Jiang, Z.X., Liang, C., 2017. Lithofacies characteristics of fine-grained sedimentary rocks in the upper submember of Member 4 of Shahejie Formation, Dongying sag and their relationship with sedimentary environment. Acta Petrol. Sin. 38 (10), 1110–1122. https://doi.org/10.7623/syxb201710002 (in Chinese).
Wu, S.T., Zhai, X.F., Yang, Z., Bale, H., Hong, Y.L., Cui, J.W., Pan, S.Q., Lin, S.H., 2019. Characterization of fracture formation in organic-rich shales-An experimental and real time study of the Permian Lucaogou Formation, Junggar Basin, northwestern China. Mar. Petrol. Geol. 107, 397–406. https://doi.org/10.1016/j.marpetgeo.2019.05.036.
Xiang, B.L., Liao, J.D., Zhou, N., Yu, Q.L., Ma, W.Y., Gao, X.W., Wang, M., 2013. Geochemical characteristic of the source rock of Lucaogou Formation in Ji174 well, Junggar Basin. Sci. Technol. Eng. 13, 9636–9640. https://doi.org/10.1016/j.petrol.2013.106364.
Xiao, X.L., Jin, X.J., Zhang, X., Liu, H.L., Jiang, Y.W., 2015. Fracture identification based on information fusion of conventional logging and electrical imaging logging. Oil Geophys. Prospect. 50 (3), 542–547. https://doi.org/10.13810/j.cnki.issn.1000-7210.2015.03.023 (in Chinese).
Xie, R.C., Zhou, W., Liu, C., Yin, S., Radwan, A.E., Lei, W., Cai, W.L., 2022. Experimental investigation on dynamic and static rock mechanical behavior, failure modes, and sequences of frequent interbedded sand and shale reservoirs. Interpretation 10 (3), 1–52. https://doi.org/10.1190/int-2021-0238.1.
Xu, S., Gou, Q.Y., Hao, F., Zhang, B.Q., Shu, Z.G., Zhang, Y.Y., 2020. Multiscale faults and fractures characterization and their effects on shale gas accumulation in the Jiaoshiba area, Sichuan Basin, China. J. Petrol. Sci. Eng. 189, 107026. https://doi.org/10.1016/j.petrol.2020.107026.
Xu, X., Zeng, L.B., Tian, H., Ling, K.G., Che, S.Q., Yu, X., Shu, Z.G., Dong, S.Q., 2021. Controlling factors of lamellation fractures in marine shales: a case study of the Fuling Area in Eastern Sichuan Basin, China. J. Petrol. Sci. Eng. 207, 109091. https://doi.org/10.1016/j.petrol.2021.109091.
Yang, Z., Hou, L.H., Lin, S.H., Luo, X., Zhang, L.J., Wu, S.T., Cui, J.W., 2018. Geologic characteristics and exploration potential of tight oil and shale oil in Lucaogou Formation in Jimusar Sag. China Petrol. Exp 23 (4), 76–85. https://doi.org/10.3969/j.issn.1672-7703.2018.04.009 (in Chinese).
Yawar, Z., Schieber, J., 2017. On the origin of silt laminae in laminated shales. Sediment. Geol. 360, 22–34. https://doi.org/10.1016/j.sedgeo.2017.09.001.
Yuan, S.Y., Su, Y.X., Wang, T.Y., Wang, J.H., Wang, S.X., 2019. Geosteering phase attributes: a new detector for the discontinuities of seismic images. IEEE Geosci 16 (1), 145–149. https://doi.org/10.1109/lgrs.2018.2866419.
Zeng, L.B., Gong, L., Guan, C., Zhang, B.J., Wang, Q.Q., Zeng, Q., Lyu, W.Y., 2022. Natural fractures and their contribution to tight gas conglomerate reservoirs: a case study in the northwestern Sichuan Basin, China. J. Petrol. Sci. Eng. 210, 110028. https://doi.org/10.1016/j.petrol.2021.110028.
Zeng, L.B., Shu, Z.G., Lyu, W.Y., Zhang, M.J., Bao, H.Y., Dong, S.Q., Chen, S.Q., Xu, J., 2021. Lamellation fractures in the Paleogene continental shale oil reservoirs in the qianjiang depression, jianghan basin, China. Geofluids 2021, 6653299. https://doi.org/10.1155/2021/665329.
Zeng, L.B., Xu, X., Ma, S.J., Bao, H.Y., Tian, H., Mao, Z., Ostadhassan, M., Dong, S.Q., Lyu, W.Y., 2024. Contribution of lamellation fractures to porosity and permeability of shales: a case study of the Jiaoshiba area in the Sichuan Basin, China.

Geoen. Sci. Eng. 232 (Part A), 212439. https://doi.org/10.1016/j.geoen.2023.212439.
Zhang, C., Zhu, D.Y., Luo, Q., Liu, L.F., Liu, D.D., Yan, L., Zhang, Y.Z., 2017. Major factors controlling fracture development in the Middle Permian Lucaogou Formation tight oil reservoir, Junggar Basin, NW China. J. Asian Earth Sci. 146, 279–295. https://doi.org/10.1016/j.jseaes.2017.04.032.
Zhang, C.J., Cao, J., Wang, Y.C., Zhi, D.M., Xiang, B.L., Li, E.T., 2022. Enrichment law of shale oil of Lucaogou Formation in jimusar sag, Junggar Basin. Acta Petrol. Sin. 43 (9), 1253–1268. https://doi.org/10.7623/syxb202209005 in Chinese.
Zhang, J.G., Jiang, Z.X., Wang, S.Q., Wang, R.Y., Zhang, Y.F., Du, W., 2021. Bedding-parallel calcite veins as a proxy for shale reservoir quality. Mar. Petrol. Geol. 127, 104975. https://doi.org/10.1016/j.marpetgeo.2021.104975.
Zhang, K.L., Wang, Z.L., Jiang, Y.Q., Wang, A.G., Xiang, B.L., Zhou, N., 2020. Effects of weathering and fracturing on the physical properties of different types of volcanic rock: implications for oil reservoirs of the Zhongguai relief, Junggar Basin, NW China. J. Petrol. Sci. Eng. 193, 107351. https://doi.org/10.1016/j.petrol.2020.107351.
Zhang, S.M., Cao, Y.C., Liu, K.Y., Jahren, J., Xi, K.L., Zhu, R.K., Yang, T., Cao, X., Wang, W., 2019. Characterization of lacustrine mixed fine-grained sedimentary rocks using coupled chemostratigraphic-petrographic analysis: a case study from a tight oil reservoir in the Jimusar Sag, Junggar Basin. Mar. Petrol. Geol. 99, 453–472. https://doi.org/10.1016/j.marpetgeo.2018.10.039.
Zhang, Y.Z., Zeng, L.B., Luo, Q., Zhang, C., Wu, H., Lyu, W.Y., Dai, Q.Q., Zhu, D.Y., 2018. Research on the types and genetic mechanisms of tight reservoir in the Lucaogou Formation in jimusar sag, Junggar Basin. Nat. Gas Geosci. 29 (2), 211–225. https://doi.org/10.11764/j.issn.1672-1926.2017.11.021.
Zhang, Z.H., Deng, J., Chen, H.Y., Yu, H.G., 2020. Self-adaptively inpainting gaps between electrical image pads according to the image fabric. Appl. Geophys. 17 (5–6), 823–833. https://doi.org/10.1007/s11770-020-0878-7.
Zhang, Z.H., Du, S.K., Chen, H.Y., Yu, H.G., 2018. Quantitative characterization of volcanic fracture distribution based on electrical imaging logging: a case study of Carboniferous in Dixi area, Junggar Basin. Acta Pet. Sin. 39 (10), 1131–1140. https://doi.org/10.7623/syxb201810005 (in Chinese).
Zhang, Z.H., Li, Z.Y., Deng, X.Q., Liao, J.B., Zheng, X.M., 2022. Multi-parameters logging identifying method for sand body architectures of tight sandstones: a case from the Triassic Chang 9 Member, Longdong area, Ordos Basin, NW China. J. Petrol. Sci. Eng. 216, 110824. https://doi.org/10.1016/j.petrol.2022.110824.
Zhang, Z.H., Yu, H.G., Chen, H.Y., Du, S.K., Li, C., 2022. Quantitative characterization of fracture-pore distribution and effects on production capacity of weathered volcanic crust reservoirs: insights from volcanic gas reservoirs of the Dixi area, Junggar Basin, Western China. Mar. Petrol. Geol. 140, 105651. https://doi.org/10.1016/j.marpetgeo.2022.105651.
Zhao, K., Du, X.B., Lu, Y.C., Xiong, S.P., Wang, Y., 2019. Are light-dark coupled laminae in lacustrine shale seasonally controlled? A case study using astronomical tuning from 42.2 to 45.4 Ma in the Dongying Depression, Bohai Bay Basin, eastern China. Palaeogeogr. Palaeoclimatol. Palaeoecol. 528, 35–49. https://doi.org/10.1016/j.palaeo.2019.04.034.
Zheng, W.H., Tian, F., Di, Q.Y., Xin, W., Cheng, F.Q., Shan, X.C., 2021. Electrofacies classification of deeply buried carbonate strata using machine learning methods: a case study on ordovician paleokarst reservoirs in Tarim Basin. Mar. Petrol. Geol. 123, 104720. https://doi.org/10.1016/j.marpetgeo.2020.104720.
Zhi, D.M., Tang, Y., Yang, Z.F., Guo, X.G., Zheng, M.L., Wan, M., Huang, L.L., 2019. Geological characteristics and accumulation mechanism of continental shale oil in Jimusar Sag, Junggar Basin. Oil Gas Geol. 40 (3), 524–534. https://doi.org/10.1016/S1876-3804(20)60103-3 (in Chinese).
Zhu, X.M., 2021. Sedimentology. Petroleum Industry Press, Beijing, p. 84 (in Chinese).